arXiv:1407.1344v1 [astro-ph.SR] 4 Jul 2014

Accepted to the Astronomical Journal

HAZMAT I: The Evolution of Far-UV and Near-UV Emission from Early M Stars [1]

Evgenya L. Shkolnik

Lowell Observatory, 1400 West Mars Hill Road, Flagstaff, AZ, 86001, USA

shkolnik@lowell.edu

and

Travis S. Barman

Department of Planetary Sciences and Lunar and Planetary Laboratory University of Arizona, Tucson AZ, 85721, USA

barman@lpl.arizona.edu

ABSTRACT

The spectral energy distribution, variability and evolution of the high-energy radiation from an M dwarf planet host is crucial in understanding the planet's atmospheric evolution and habitability and in interpreting the planet's spectrum. The star's extreme-UV (EUV), far-UV (FUV) and near-UV (NUV) emission can chemically modify, ionize, and erode the atmosphere over time. This makes determining the lifetime exposure of such planets to stellar UV radiation critical for both the evolution of a planet's atmosphere and our potential to characterize it. Using the early M star members of nearby young moving groups (YMGs), which sample critical ages in planet formation and evolution, we measure the *GALEX* NUV and FUV flux as a function of age. The median UV flux remains at a "saturated" level for a few hundred million years, analogous to that observed for X-ray emission. By the age of the Hyades Cluster (650 Myr), we measure a drop in UV flux by a factor of 2–3 followed by a steep drop from old (several Gyrs) field stars. This decline in activity beyond 300 Myr follows roughly t^{-1}. Despite

[1]Based on observations made with the NASA Galaxy Evolution Explorer. *GALEX* was operated for NASA by the California Institute of Technology under NASA contract NAS5-98034.

this clear evolution, there remains a wide range of 1–2 orders of magnitude in observed emission levels at every age. These UV data supply the much-needed constraints to M dwarf upper-atmosphere models, which will provide empirically-motivated EUV predictions and more accurate age-dependent UV spectra as inputs to planetary photochemical models.

Subject headings: stars: exoplanet hosts, stars: late-type, activity

1. Introduction

The conditions inside the circumstellar disks of M dwarfs provide a favorable environment for the formation of low-mass planets close to the star (Wu & Lithwick 2013), as indicated by the ∼50% small planet occurrence rate around M dwarfs in the habitable zone (HZ; ≈0.1–0.4 AU; Bonfils et al. 2013; Kopparapu 2013; Dressing & Charbonneau 2014). This implies that most of the planets in our galaxy, including those in the HZ, orbit M dwarfs as these low-mass stars make up 75% of the total stellar population (Bochanski et al. 2008). In fact, M dwarfs are proposed (Tarter et al. 2007; Scalo et al. 2007) to be the most sought-after candidate planet-hosts as they are the most amenable to follow-up observations, including the first potentially habitable planets to be spectroscopically characterized, probably by *JWST* transit transmission observations (Deming et al. 2009). In the next few years, many more planets will be identified around bright M stars by both ground- and space-based instruments including TESS, CARMENES, SPIROU and NGTS (Ricker et al. 2014; Quirrenbach et al. 2012; Delfosse et al. 2013; Wheatley et al. 2014, respectively), for which the incident stellar high-energy spectrum will be critical to understanding the planets' atmospheres.

The EUV and FUV spectrum of the star dominates atmospheric photochemistry of planets by affecting composition, ionization, and stability (e.g., Kasting et al. 1993; Lichtenegger et al. 2010; Segura et al. 2010), including the photodissociation of molecules important to surface habitability, e.g. H_2O, CH_4, and CO_2. The UV increases the generation of surface-shielding hazes in reducing atmospheres (Zerkle et al. 2012) and ozone (O_3) in oxidizing atmospheres (Segura et al. 2003, 2005), both of which can strongly affect the observed spectrum. Recently, Robinson et al. (2014) showed that Titan's high altitude haze affects its transit spectrum and severely limits the atmospheric depths which can probed by such data. Observations of exoplanet transit transmission spectroscopy (Bean et al. 2011; Kreidberg et al. 2014) are showing that hazes in planets around M dwarfs might in fact be quite common, probably generated by the star's UV. The ratio of the FUV to NUV flux can increase the detectability of biologically generated gases (Segura et al. 2005), but may also lead to the formation of

abiotic oxygen and ozone (Tian et al. 2014; Domagal-Goldman et al. 2014) producing a false-positive biosignature for oxygenic photosynthesis. And the NUV flux can photodissociate diagnostic molecules such as sulfur dioxide (SO_2) and ammonia (NH_3).

The EUV stellar radiation (100–900Å) can be particularly damaging as it photoionizes, heats and inflates a planet's upper-atmosphere making it vulnerable to massloss (Koskinen et al. 2010). Two aeronomical studies have explored the potential for massloss by applying a wide range of EUV emission. Lammer et al. (2007) conclude that the atmosphere of an unmagnetized telluric planet can be completely eroded in its first Gyr by high M dwarf activity levels and corresponding coronal mass ejections. On the other hand, Tian (2009) find that the atmosphere of a super-Earth is stable even around very active M dwarfs.

Direct observations of the EUV spectral range is currently impossible since the completion of the EUVE space mission and its obscuration due to interstellar neutral hydrogen. Estimating EUV fluxes from existing M dwarf model atmospheres is also not feasible because current models lack any prescription for the lowest density regions of the upper-atmosphere, namely the chromosphere, transition region and corona, causing severely under-predicted emission at all UV wavelengths (e.g. Woitke et al. 2011 and Figure 1).

Two empirical options remain: extrapolate to EUV wavelengths from either X-ray or UV observations. Lecavelier Des Etangs (2007) and Sanz-Forcada et al. (2011) estimate EUV fluxes in known, old, solar-type planet hosts using coronal models fits to X-ray spectra. The latter paper noted that the contribution to the EUV flux from the transition region is unknown because of the lack of FUV spectra. Since both the FUV and the EUV spectral ranges are filled by emission lines formed at upper-transition region and lower-coronal temperatures (e.g. as show for the Sun by Kretzschmar et al. 2009), there is also promise to approaching the EUV predictions from the FUV (Linsky et al. 2014). Interpolating between X-ray and FUV data for a given star is also an option, but as discussed in Section 4.1, it is problematic with the currently available data sets.

Photochemical models calculated for the atmospheres of all exoplanets, from Earths to Jupiters (e.g., Segura et al. 2010; Line et al. 2010; Kaltenegger et al. 2011; Hu et al. 2012; Kopparapu et al. 2012; Moses et al. 2013) require realistic input stellar fluxes, and are at the moment limited to using solar data in most cases (e.g. Fontenla et al. 2009). For M dwarfs, there exist very few UV spectra to use. Walkowicz et al. (2008) collected very low-resolution Hubble Space Telescope (*HST*) NUV data of 33 M dwarfs. More recently France et al. (2013) secured *HST* high-resolution FUV and NUV spectra of six old M dwarf planet hosts with a wide range of spectral types (M1–M6). These are providing valuable initial inputs to planetary photochemical models (Miguel & Kaltenegger 2014; Tian et al. 2014), however, the full history of a planet's UV exposure is impossible to predict from a single observation.

It is critical to study stars spanning a wide range of ages with many stars at each age to help mitigate the effects of flaring from a single star and provide a more accurate mean level and range of UV activity for M stars at a given mass and age.

It is well-known that all types of stars are more active in their youth, with a progressive decline with age. The rate of decline in stellar X-ray emission was shown to vary with stellar mass, with M dwarfs remaining X-ray active (and rotating faster) much longer than FGK stars (Pizzolato et al. 2003; Preibisch & Feigelson 2005; Selsis et al. 2007). The Galaxy Evolution Explorer (*GALEX*) provides a new data set with which to study the broadband FUV and NUV emission from many more stars, and at much greater distances ($\gtrsim$100 pc) than previously possible (Findeisen & Hillenbrand 2010; Shkolnik et al. 2011), including 65% of the known planet hosts (Shkolnik 2013). Here, we detail the UV evolution of early Ms, from 10's to 100's to 1000's of Myrs, sampling critical ages in planet formation and evolution (e.g., Mandell et al. 2007), extending the work of Findeisen et al. (2011) for more massive stars to M dwarfs. This work represents the first results of the HAZMAT (HAbitable Zones and M dwarf Activity across Time) program, providing the empirical guidance needed to build new M dwarf upper-atmosphere models (Peacock, Barman & Shkolnik, in preparation), to characterize of the full-UV spectrum, including the EUV and Lyman α, for the stars that are the most common planet hosts. These models will provide a grid of input spectra to planetary atmospheric photochemical models to study the impact of M dwarf UV evolution on planetary atmospheres, including constraining planet atmospheric evaporation which is completely dependent upon the stellar EUV fluxes.

The target stars in this study consist of the low-mass members of the nearby young moving groups (YMGs), which provide the most accurate stellar ages available for dispersed M stars. The YMGs are TW Hydra at 10 Myr, β Pic at 12 Myr,[1] Tuc-Hor at 40 Myr, AB Dor at 100 Myr, Ursa Major at 300 Myr, and the Hyades cluster at 650 Myr. Each star has been shown to be kinematically linked (using 3-D space velocities) to one of these YMGs (e.g., Zuckerman & Song 2004; Torres et al. 2008; Shkolnik et al. 2011, 2012; Kraus et al. 2014), and also exhibits independent youth indicators such as elevated stellar activity levels, low gravity, and possibly lithium absorption (e.g. Shkolnik et al. 2009). We complement the study with the old population of M stars within 10 pc, which has an average age of $\sim$5 Gyr.

[1]Binks & Jeffries (2013) places the β Pic YMG at 21$\pm$4 Myrs.

2. *GALEX* NUV and FUV Photometry

The *GALEX* satellite was launched on April 28, 2003 and imaged approximately 3/4 of the sky simultaneously in two UV bands: FUV 1350–1750 Å and NUV 1750–2750 Å. For stars hotter than about 5250 K, the flux in the *GALEX* bandpasses is made up predominantly from continuum emission (Smith & Redenbaugh 2010) with additional flux provided by strong emission lines (C IV, C II, Si IV, He II) originating from the upper-atmosphere. Cooler stars have FUV and NUV fluxes strongly dominated by stellar activity (e.g. Robinson et al. 2005; Welsh et al. 2006; Pagano 2009), making *GALEX* an excellent tool with which to study stellar activity in low-mass stars lying within ∼150 pc (e.g. Findeisen & Hillenbrand 2010; Shkolnik et al. 2011). The *GALEX* FUV bandpass does not include the chromospheric Lyman α line (1216 Å), which Linsky et al. (2014) measure to be as bright as the entire 1200–3200 Å spectrum of M dwarfs (France et al. 2013), but direct observations of the Lyman α emission are very difficult due to interstellar hydrogen absorption and geocoronal emission. Linsky et al. (2013) showed that intrinsic Lyman α correlates with other emission lines, including C IV, which contributes ∼50% of the *GALEX* FUV flux (Robinson et al. 2005; Welsh et al. 2007).

In addition to a medium and a deep imaging survey (MIS, DIS), covering 1000 and 100 square degrees, respectively, the *GALEX* mission has produced an All-sky Imaging Survey (AIS), all of which is archived at the Barbara A. Mikulski Archive for Space Telescopes (MAST). The angular resolutions are 6.5″ and 5″ in the FUV and NUV, respectively, across a 1.25° field of view. The full description of the instrumental performance is presented by Morrissey et al. (2005).[2] The fluxes and magnitudes averaged over the entire exposure were produced by the standard *GALEX* Data Analysis Pipeline (ver. 4.0) operated at the Caltech Science Operations Center (Morrissey et al. 2007). The data presented in this paper made use of the sixth data release (GR6/7), which includes the three surveys plus publicly available data from Guest Investigator (GII) programs.

The *GALEX* pipeline performs aperture photometry using several sizes. We chose the "aper_7" which has a radius of 17.3″. This relatively large aperture requires the least aperture correction (0.04 mags in both the in NUV and FUV bandpasses)[3] and encompasses the full range of possible PSFs, even near the edges of the images where the PSF is elongated. In

[2]One can query the *GALEX* archive through either CasJobs (http://mastweb.stsci.edu/gcasjobs/) or the web tool GalexView (http://galex.stsci.edu/galexview/).

[3]See Table 1 of http://www.galex.caltech.edu/researcher/techdoc-ch5.html. Note Morrissey et al. (2007) quote a required aperture correction of 0.07 mags. Either way the effect is very small compared to the uncertainties and the large differences in flux between targets.

order to exclude the severest edge effects, we limit our detections to those within 0.59° from the center of the 1.25°-wide image.

We cross-correlated the published early-M YMG members as of April 2014 and old field stars with masses ranging from ≈0.3–0.65$M_\odot$ with the *GALEX* archive using a 12″ search radius (Figure 2) resulting in 215 observed stars. We exclude lower mass targets at this time because there are very few known in YMGs, and since such fully-convective stars have been shown to exhibit much more erratic flare activity (e.g. Reiners & Basri 2009), it would be difficult to make statistical conclusions about the evolution of their stellar activity with so few.

Kraus et al. (2014) showed that many of these young stars originally selected for their youth using high UV emission (e.g. Shkolnik et al. 2011; Rodriguez et al. 2011) are not biased towards only the high-activity stars, but rather the vast majority of all YMG members are indeed very active. For the old sample of stars within 10 pc that have very high proper motions, we conducted the search with proper-motion-corrected coordinates using the dates of the *GALEX* images. Fluxes are calculated from the reported flux densities using the effective wavelengths of 2267Å and 1516Å for the NUV and FUV bandpasses, respectively.[4] Given that our sample is mostly within 50 pc, we do not include the effects of UV extinction as Findeisen et al. (2011) showed that the effects are insignificant even out to 250 pc.

Since not all of the stars have trigonometric parallaxes, nor are published bolometric corrections for M dwarfs precise, we analyze the UV fractional flux densities relative to the 2MASS J magnitude, i.e. F_{FUV}/F_J and F_{NUV}/F_J.[5] A comparison of fractional flux densities to stellar surface flux for those stars with parallaxes is shown in Figure 3.

Table 1 lists all of our targets observed by *GALEX*, their coordinates, published spectral types (SpTs), 2MASS J band magnitudes, and UV flux densities.[6] In the NUV, 95% the stars observed by *GALEX* were detected. In the FUV, 72% of Tuc-Hor members, 35% of the Hyades members, and 52% of the old stars were detected. For those not detected, we

[4]These values are taken from Table 1.1 of http://galexgi.gsfc.nasa.gov/docs/galex/Documents/ERO_data_description_2.htm. Morrissey et al. (2007) report slightly different values for effective wavelengths: 2315.7 Å and 1538.6 Å.

[5]These flux densities are calculated using Janskys. In order to convert these ratios to quantities based in flux units of erg s^{-1} cm^{-2}, multiplicative factors of 10.98 and 13.41 can be applied to the F_{FUV}/F_J and F_{NUV}/F_J values, respectively.

[6]We independently measured the FUV and NUV fluxes of all the stars, including the old stars that overlap with those in Stelzer et al. (2013). We noticed an error in Stelzer et al. (2013)'s values which they corrected in Stelzer et al. (2014).

calculated 1-σ upper limits by determining the median flux error for a given exposure time for those stars that were detected. These are shown in Figure 4. We identified the targets with known stellar companions within 17.3″, which may increase the observed flux either by having an active secondary or through the tidal spin-up of primary. It is evident that the TW Hydra Association (TWA; 10 Myr) is so far the best-surveyed YMG for companions (64% of our TWA sample are known binaries), and given that our knowledge of the other YMGs is not nearly as complete, we have chosen to include the known binaries in our analysis, with the assumption that the binary fraction in other moving groups is likely to be comparable to TWA's. Including the known binaries does not significantly affect the final conclusions of this paper.

3. Evolution of the Photospheric UV Emission

Commonly used M dwarf photospheric models have temperature structures that do not include rises characteristic of chromospheres, transition regions, or coronae and, therefore, the term "photospheric" (or "photosphere-only") is used here when referring to fluxes from such models. In order to test the evolution of the photosphere and its corresponding effects on the observed changes in UV flux with time, we calculated the photospheric flux using the PHOENIX stellar atmosphere models (Hauschildt et al. 1997; Short & Hauschildt 2005) convolved with the relevant NUV, FUV and J band normalized transmission curves. Figure 5 shows the evolution of the photospheric fractional flux density for a range of stellar masses (0.3, 0.4, 0.5, 0.6, and 0.7 $M_{\odot}$).

Using the stellar age and published SpT, we derive a $T_{\rm eff}$ and mass using the Baraffe et al. (1998) models and measure the corresponding photospheric flux from the PHOENIX models for each star in our sample. In the NUV, the photospheric flux comprised $< 5\%$ of the observed flux in most stars, except for the oldest M dwarfs in which the photospheric contribution peaks at 40%. In the FUV, the photosphere is negligible, comprising only 0.005% or less of the observed flux. The ratios of the photospheric to observed flux densities as a function of $T_{\rm eff}$ are shown in Figure 6 and as a function of age in Figure 7. A trend with $T_{\rm eff}$ in the FUV (left) plot of Figure 6 is evident, which is not seen in the NUV (right) plot. This difference is due to the steeper drop in photospheric FUV flux compared to the NUV with decreasing $T_{\rm eff}$. For all stars we subtract the photospheric contribution from the observed *GALEX* flux densities providing the excess emission, $(F_{FUV}/F_J)_{exc}$ and $(F_{NUV}/F_J)_{exc}$, as a measure of pure upper-atmosphere activity.

By comparing the absolute J band magnitudes of the old sample (all of which have published trigonometric distances) to the model predictions, we find a mean absolute deviation

of 0.4 mag, corresponding to a 31% uncertainty in model J-band flux density. Given that we are subtracting a relatively small value of fractional photospheric FUV and NUV flux from the observed flux, this uncertainty is not significant in the quantities reported.

4. Results

4.1. Correlations Between Stellar Activity Diagnostics

X-ray emission is ubiquitous among low-mass stars and is indicative of active stellar upper-atmospheres throughout their lifetimes, e.g. 94% of all K and M dwarfs within 6 pc exhibited detectable X-ray emission as observed by *ROSAT*[7] (Schmitt et al. 1995). Fractional X-ray luminosities have also been shown to be "saturated" across a wide range of spectral types, Hα equivalent widths, and ages at the value of $\log(L_X/L_{\rm bol}) \sim -3$, with the bulk of the dispersion in both field and cluster samples between $\log(L_X/L_{\rm bol})$ of –2 and –4 primarily due to variations in stellar rotation (Stauffer et al. 1997; Delfosse et al. 1998; Jackson et al. 2012).

Correlations among stellar activity indicators are useful in understanding the formation mechanisms of emission features, energy distributions in the stellar atmosphere, and to allow one activity diagnostic to act as a proxy for another. Should observations of X-ray, FUV and NUV fluxes correlate with the EUV, then more accurate EUV flux estimates can be obtained. At the moment, there are fewer than 10 M dwarfs (with a wide range of stellar masses) for which EUV data exist in the archives making the robust connection between EUV and X-ray and between EUV and FUV/NUV impossible for a wide range of stellar masses and ages. Interpolating between X-ray and FUV fluxes is yet another possible route, assuming the line formation mechanisms are the same in all three wavelength ranges and correlations are observed. Mitra-Kraev et al. (2005) observed 5 dMe stars (the classic flare stars AT Mic, AU Mic, EV Lac, UV Cet and YZ CMi) simultaneously in X-ray and UV wavelengths. They find a significant correlation from which they conclude that stellar chromospheres and coronae are both continuously heated by common impulsive energy release processes, at least for very active M dwarfs.

In order to compare X-ray and UV data, we cross-referenced the sample of YMG M stars against the *ROSAT* All-Sky Survey Bright Source Catalog and Faint Source Catalog (Voges et al. 1999, 2000). Our query was limited to a search radius of 38″ around the 2MASS

[7]The Röntgensatellit (*ROSAT*) was a joint German, US and British X-ray observatory operational from 1990 to 1999.

coordinates, the 3σ positional error determined by Voges et al. (1999). For the field sample, the search radius was increased to accommodate the very high proper motion stars. The empirically-calibrated X-ray flux (F_X) in erg s^{-1} cm^{-2} was calculated using the count-rate conversion equation of Schmitt et al. (1995).

Figure 8 shows a correlation between F_{FUV}/F_J and F_{NUV}/F_J across the wide range of fluxes with a correlation coefficient R=0.94. Comparing the F_X/F_J to $(F_{FUV}/F_J)_{exc}$ and $(F_{NUV}/F_J)_{exc}$, significant correlations exist using the full range of fluxes ($R = 0.85$), which covers 3 orders of magnitude in X-ray and UV fluxes. As seen in Figure 9, the correlation is primarily defined by two clusters: one group of low-emitters and one of high-emitters (roughly old and young stars, respectively). When focusing on only the strong and weak emitters, the correlations weaken ($R = 0.36$ and 0.18, respectively, for the NUV and $R =$ 0.42 and 0.49 for the FUV). Results of the regression analyses are summarized in Table 2. In almost all cases, the NUV and FUV observations were taken simultaneously by *GALEX*, but the *ROSAT* X-ray observations were collected years earlier. It is most likely that the non-simultaneity of the observations contributes to the lack of a correlation due to the short-term flaring distribution and long-term activity cycles.

4.2. Intra-age Stellar Variability

We observe a span of 1–2 orders of magnitude in UV activity at each age as seen in Figure 10. With the many more FUV upper limits in the Hyades and old field samples, it is likely that the full span of emission levels is even larger at these older ages. Some of this wide range in UV activity among the field stars is due to the uncertain stellar ages, from 1 to 10 Gyr. The large spread in measured rotation periods of M stars at both young and old ages (e.g. Irwin et al. 2011 and reference therein) must also contribute to the UV flux variation, although Pizzolato et al. (2003) showed that young stars with saturation-level X-ray emission, do not follow the expected rotation-activity relation seen in older stars. Short transient events such as flares must also contribute. Welsh et al. (2007) observed such events in 3% of old field M dwarfs found in the the *GALEX* archive within a single 1500-s exposure, while *HST* UV spectra of a few old M dwarf planet hosts revealed a variety of flare activity, with variability amplitudes ranging from factors of 2 to 10 on timescales of 100 – 1000 seconds (France et al. 2013). For young Ms, larger and more frequent flares are expected.

4.3. Activity Drop with Age

It has been well-established that the chromospheric activity and coronal emission of FGKM stars steadily decreases with age due to the reduced dynamo production of magnetic fields as the star spins down. Unlike the spin-down time scale for higher-mass stars (<1 Gyr; e.g. Skumanich 1972), the spin-down time-scales for field M dwarfs range from 1 to 10 Gyr, taking longer with decreasing stellar mass (Delfosse et al. 1998; Irwin et al. 2011). The angular momentum evolution of early-Ms appears to be the most dramatic between 10 and 300 Myr old, increasing rotation rates until about 100 Myr and then starting a slow decline (Irwin et al. 2011; Kidder, Shkolnik & Skiff, in preparation).

Using the relatively accurate ages of the YMG members, we map the evolution of the high FUV and NUV emission as a function of time. Figures 11 and 12 shows no significant evolution in both the FUV and NUV emission from 10 to a few hundred Myrs with a decline beginning by 650 Myr followed by a sharp drop by two orders of magnitude in the old sample. This is similar behavior to X-ray data (Preibisch & Feigelson 2005). Güdel et al. (1997) showed a $t^{-1.5}$ decline in X-ray luminosity for solar mass stars beyond 1 Gyr. A slower decrease of $L_X \propto t^{-1}$ is predicted by Feigelson et al. (2004) for lower-mass stars, but they measured $L_X \propto t^{-2}$. With the few points they had, they could not rule out a shallower decline. We measure a drop in NUV and FUV fractional flux[8] to be proportional to $t^{-0.84\pm0.09}$ and $t^{-0.99\pm0.19}$, respectively, for ages $\gtrsim$200 Myr, with a decline in the fractional X-ray flux of our sample to be $t^{-1.36\pm0.32}$. (See Table 2.) The consistency between the X-ray and the FUV implies that, at least qualitatively, we can draw similar conclusions for the EUV – i.e. a saturation level of emission until a few hundred millions of years and a reduction in flux with age afterward following roughly t^{-1}. The decline in the NUV is notably shallower.

Comparing the median excess fluxes of the youngest (TWA + β Pic) to the oldest stars reveals a drop in emission by factors of 65, 30, and 20 in the X-ray, FUV and NUV, respectively,[9] implying that the decline in flux with age may steepen with shorter wavelength. Claire et al. (2012) have shown a similar change with wavelength for a small sample of Sun-like stars. Interpolating between the X-ray and NUV results to assess the decline in EUV flux is limited to between ≈30 to ≈65 due to the very large scatter in activity levels at each age of the sample.

---

[8]Note that due the high fraction (42%) of FUV upper limits in the old sample, we use predicted values of the FUV based on the correlation found in Figure 8.

[9]Using the upper limits rather than predicted FUV values, the young-to-old ratio is 26, rather than 30.

5. Summary

Using archived *GALEX* photometry, we analyzed the evolution of the FUV and NUV emission in early M stars. Our sample consisted of 215 stars at ages of 10, 12, 40, 100, 300 and 650 Myr, probing critical planet formation and evolution time scales. These stars are confirmed members of known YMGs, the Hyades cluster and the old field sample within 10 pc. Ninety-five percent of the targets observed by *GALEX* in the NUV were detected, while 184 of the stars observed in the FUV had a 68% detection rate.

We used current (i.e. photosphere-only) PHOENIX models to calculate the photospheric contribution to the two *GALEX* bandpasses and subtracted it from the observed quantities to study the evolution of the stellar activity originating from the chromosphere, transition region and corona. The main results from the analysis of the X-ray, FUV and NUV flux emitted from these M stars are:

• In most cases, the photospheric flux in the NUV bandpass contributes less than 5% of the total observed flux, except for the oldest M dwarfs, in which the photospheric contribution peaks at ∼40%. In the FUV, the photosphere contributes at most 0.005% of the observed flux.

• A range of 1 to 2 orders of magnitude in UV activity is observed at each age. Stellar rotation, unknown binarity, long-term activity cycles and short-term flaring all likely contribute to this wide range, highlighting the difficulty of extending single activity measurements of M dwarfs at UV or X-ray wavelengths to the EUV.

• The X-ray and UV fluxes correlate over a broad range of activity levels, defined by two groups: high and low emitters. Within each group there is only a weak correlation, likely due to the non-simultaneity of the UV and X-ray observations.

• Qualitatively, the FUV and NUV excess flux densities decay in a similar fashion to X-ray results, with a high saturation level from 10 Myr until a few hundred Myrs. By the age of the Hyades at 650 Myr, we measure a drop in excess flux, after which it plummets at the old ages of the field sample. Without these measurements at each individual age, a single power-law fit to just the TWA and oldest stars, as done by Stelzer et al. (2013), underestimates the UV emission from M stars by a factor of 3–5 over many hundreds of Myrs.

• The median excess fractional fluxes at each age show a reduction in FUV and NUV by factors of 30 and 20, respectively, from young to old ages. Combining this with an observed drop in X-ray by a factor of 65 suggests that the median reduction in flux with age may steepen with shorter wavelength, and that the drop in EUV flux most likely falls in between.

The reported FUV and NUV fluxes provide the empirical guidance needed to build new M dwarf upper-atmosphere models (Peacock, Barman & Shkolnik, in preparation), to characterize of the full-UV spectra, including the EUV and Lyman α, for the stars that are the most common planet hosts. These models will provide a grid of input spectra to planetary atmospheric photochemical models to study the impact of M dwarf UV evolution on planetary atmospheres.

E.S. would like to thank V. Meadows for stimulating discussions, B. Stelzer and the referee, L. Fossati, for helpful comments on the manuscript, and S. Neff and the *GALEX* team for answering questions about the archive. This material is based upon work supported by the NASA/GALEX grant program under Cooperative Agreement No. NNX12AC19G issued through the Office of Space Science, and through generous funding to Lowell Observatory by D. Trantow and M. Beckage. This research has made use of the VizieR catalogue access tool, CDS, Strasbourg, France (Ochsenbein et al. 2000) and the Mikulski Archive for Space Telescopes (MAST). STScI is operated by the Association of Universities for Research in Astronomy, Inc., under NASA contract NAS5-26555. Support for MAST for non-HST data is provided by the NASA Office of Space Science via grant NNX13AC07G and by other grants and contracts.

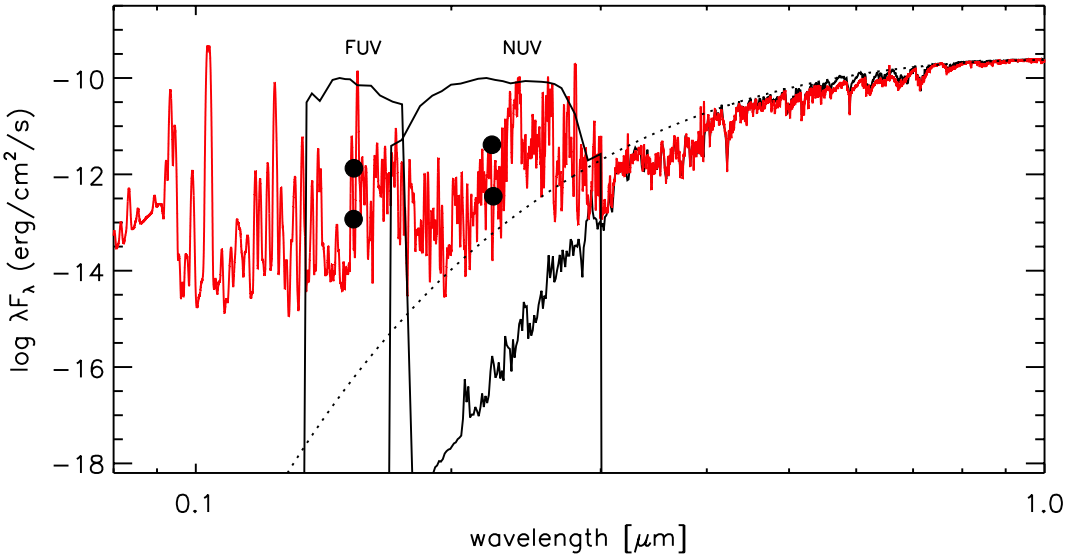

Fig. 1.— Model spectra for a 50-Myr old star with $T_{\rm eff}$=3500 K: photosphere only model (solid black curve), the photosphere + upper-atmosphere model (red curve), and a 3500-K blackbody (black dashed curve). The data points are *GALEX* fluxes for a young (higher points) and old star (lower points) with the same $T_{\rm eff}$.

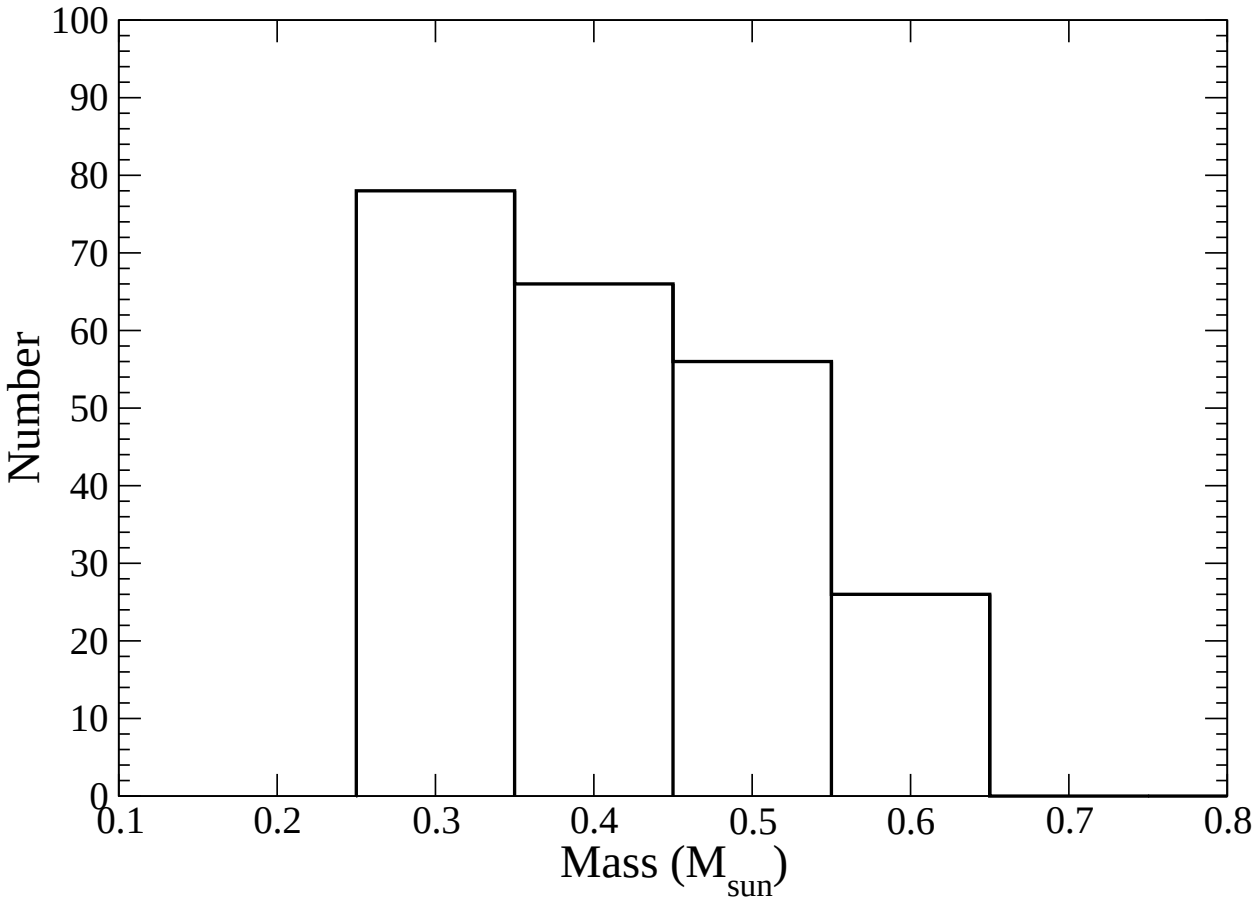

Fig. 2.— Stellar mass distribution of the sample using literature SpTs and Baraffe et al. (1998) models for a given stellar age.

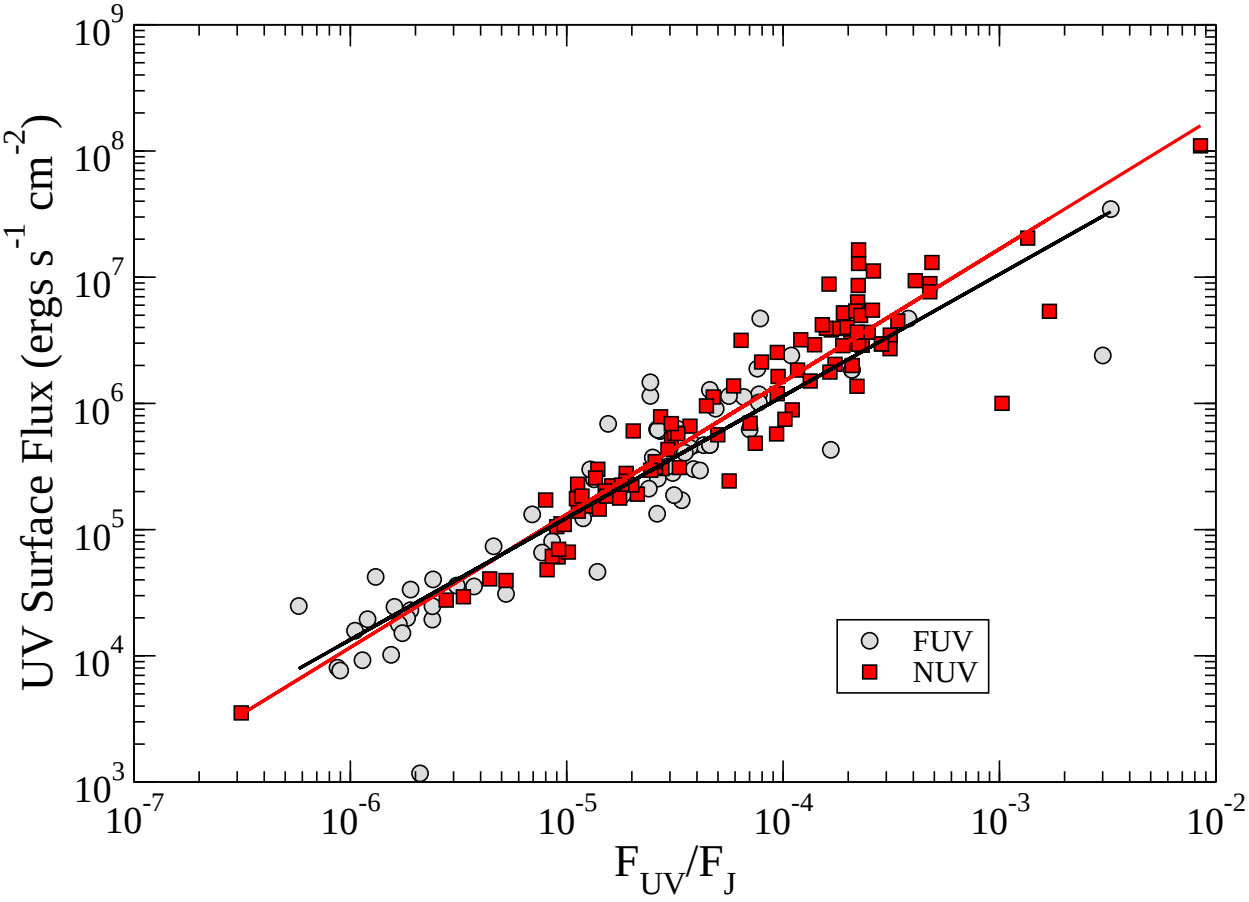

Fig. 3.— FUV and NUV fractional flux densities plotted against the surface flux for those stars with trigonometric parallaxes.

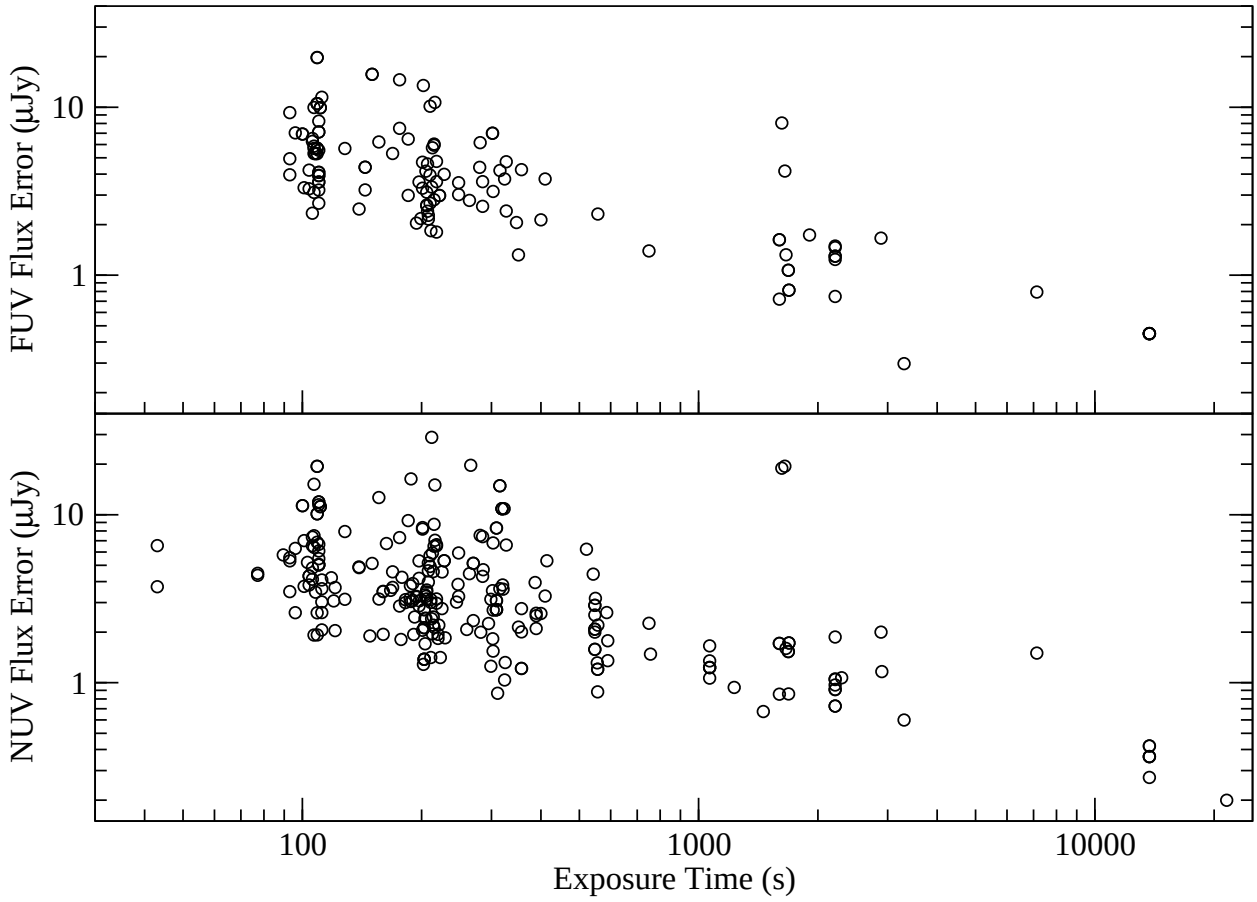

Fig. 4.— Reported flux errors for the FUV (top) and NUV (bottom) detections.

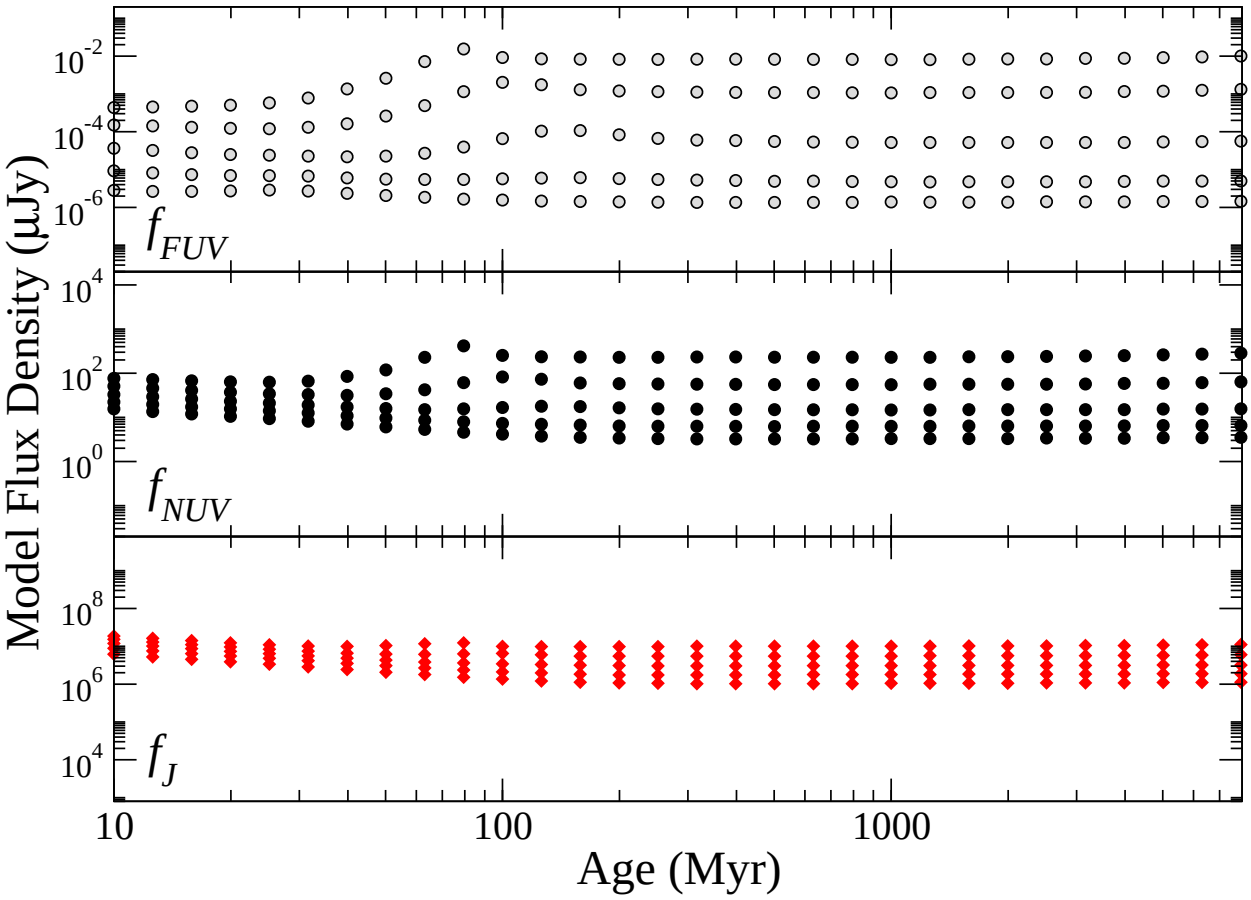

Fig. 5.— The photospheric FUV, NUV and J band flux density as a function of age for masses M_*=0.3, 0.4, 0.5, 0.6 and 0.7 $M_\odot$ (low to high).

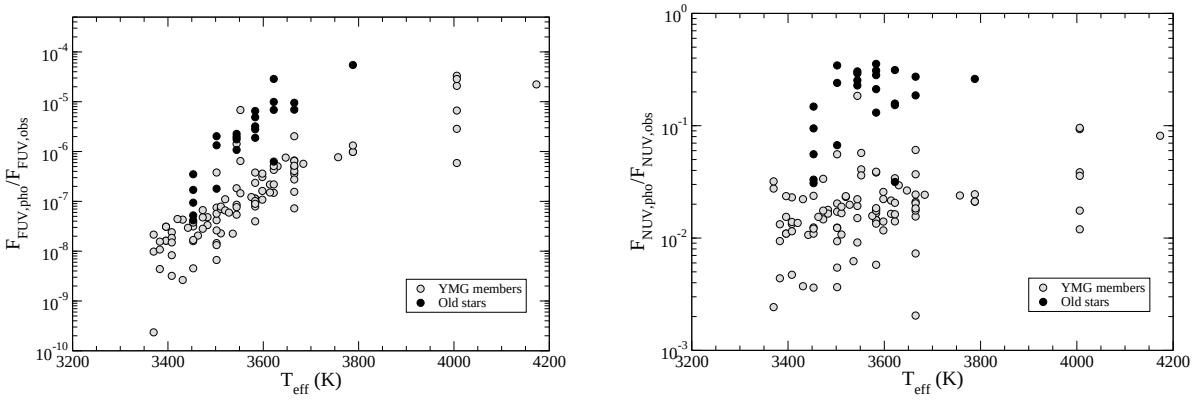

Fig. 6.— The fraction of the observed FUV (left) and NUV (right) flux density contributed by the stellar photosphere as a function of stellar effective temperature.

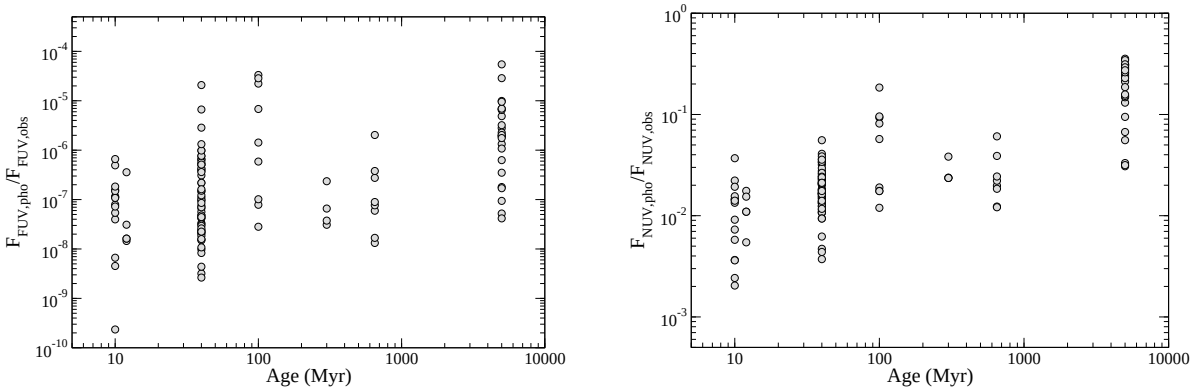

Fig. 7.— The fraction of the observed FUV (left) and NUV (right) flux contributed by the stellar photosphere as a function of stellar age.

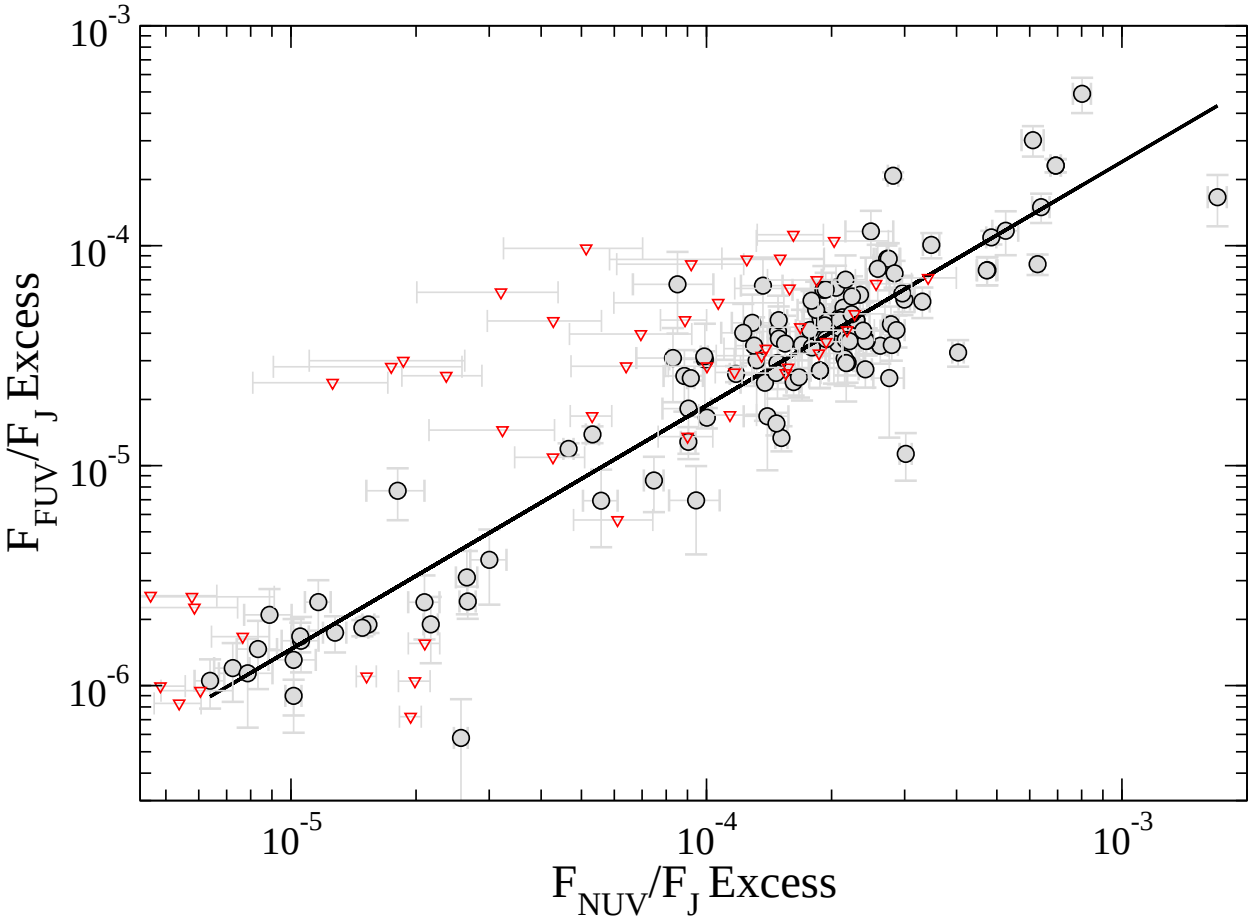

Fig. 8.— The *GALEX* NUV and FUV excess fractional flux density for stars in our sample with detections in both bandpasses (grey dots). The solid line is a regression fit to the detections with a slope of 1.11±0.04. The red triangles are FUV upper limits with NUV detections.

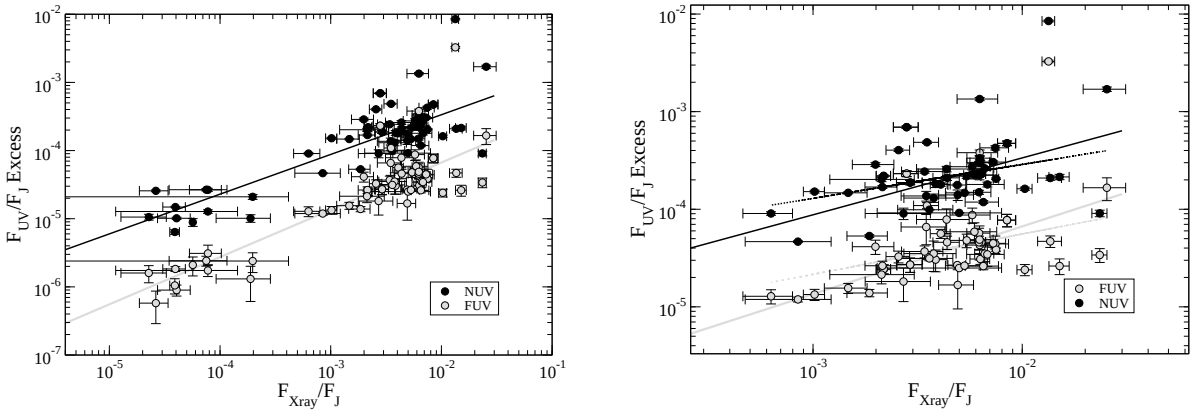

Fig. 9.— The excess NUV and FUV fractional flux density plotted against the X-ray fractional flux from *ROSAT*. The coefficients of the regression lines are listed in Table 2. The right plot focuses on the high-activity cluster of points with correlations from the left plot (solid line) plus the regression lines fit only to the shown high flux data (dashed line), showing a much weaker correlation between UV and X-ray data.

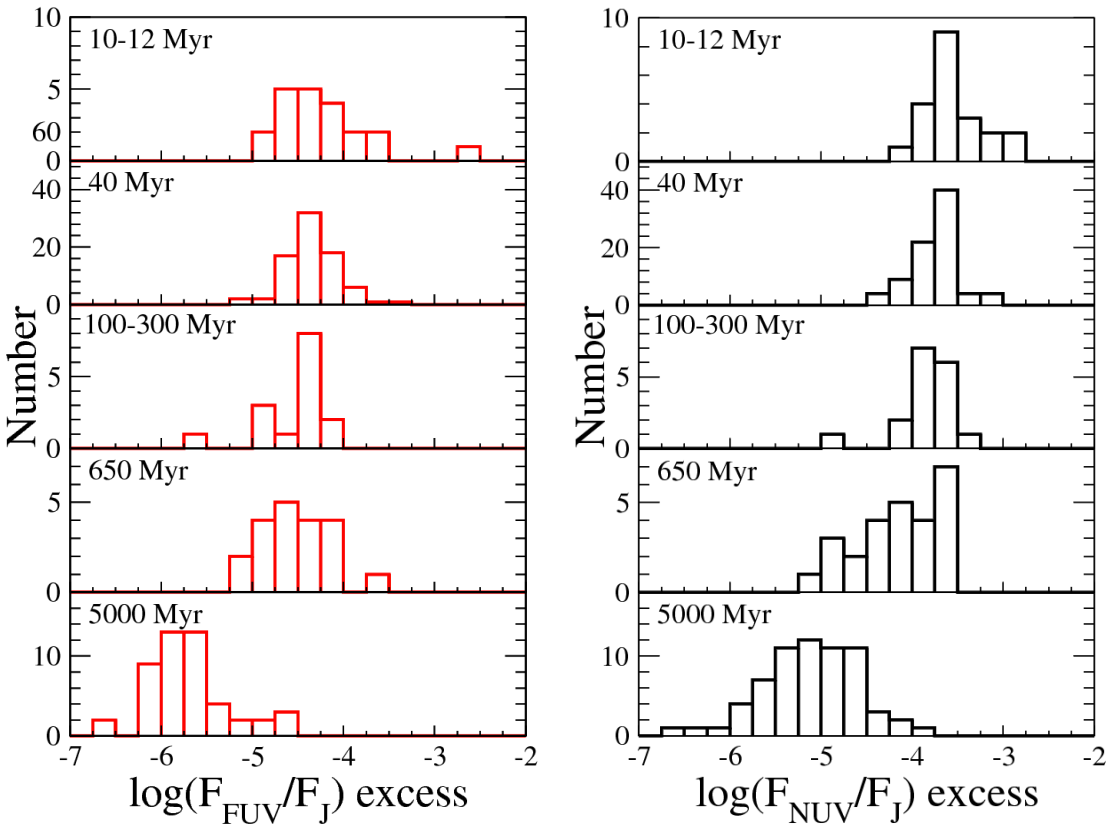

Fig. 10.— Histogram of excess fractional FUV (left) and NUV (right) flux densities including upper limits.

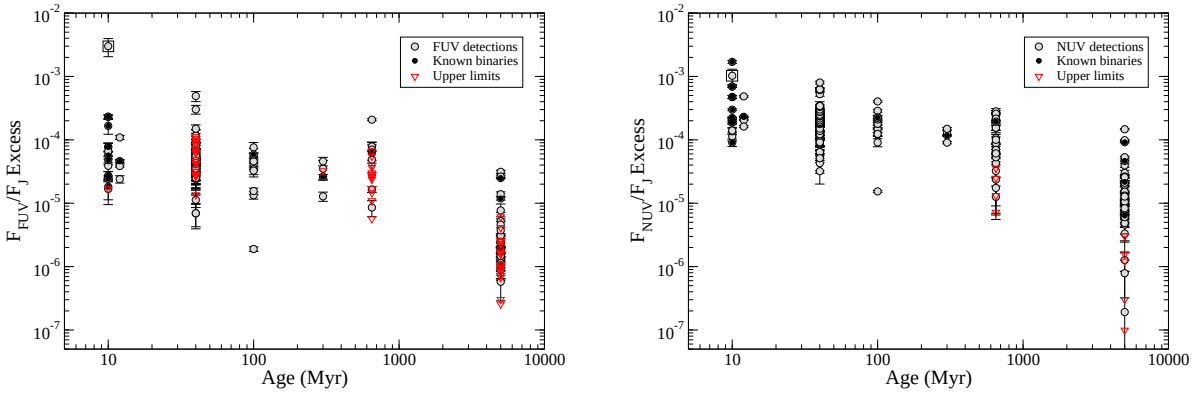

Fig. 11.— The excess FUV (left) and NUV (right) fractional flux density, where the photospheric flux from the appropriate model is subtracted from the observed flux, plotted as a function of stellar age. The boxed data point is the accreting star TWA 31.

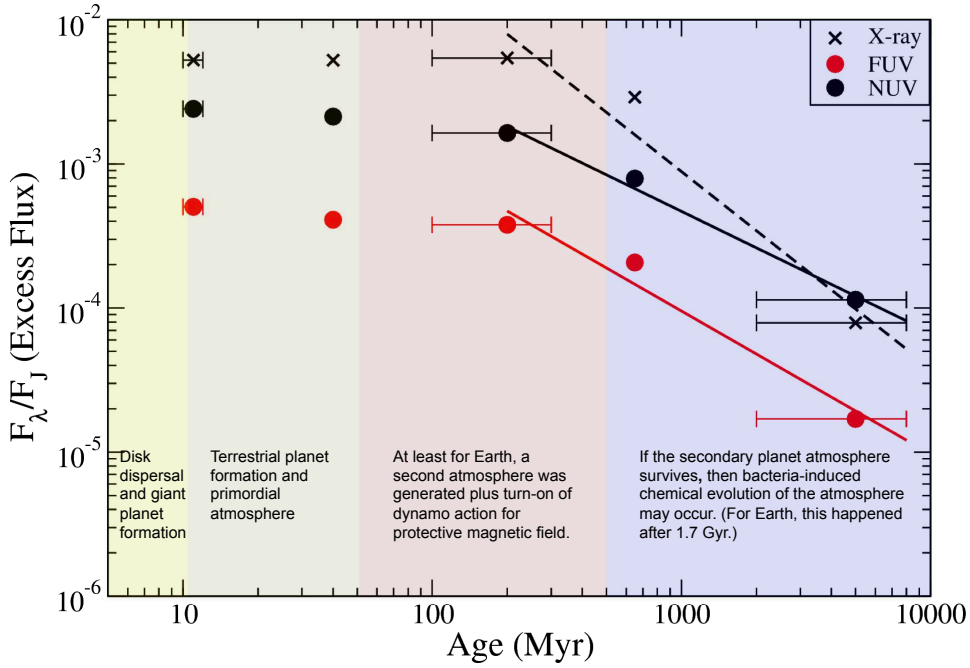
X-ray
FUV
NUV
Disk dispersal and giant planet formation
Terrestrial planet formation and primordial atmosphere
At least for Earth, a second atmosphere was generated plus turn-on of dynamo action for protective magnetic field.
If the secondary planet atmosphere survives, then bacteria-induced chemical evolution of the atmosphere may occur. (For Earth, this happened after 1.7 Gyr.)
F_λ/F_J (Excess Flux)
Age (Myr)
10
100
1000
10000

Fig. 12.— Median X-ray, FUV and NUV excess fluxes (not flux densities), including upper limits, as a function of stellar age. The FUV median values for the Hyades cluster and the old sample are comprised of 65% and 42% upper limits, respectively. Using the correlation in Figure 8, we predicted the FUV values for those with upper limits. The coefficients of the power-law fits to the three bandpasses are listed in Table 2.

REFERENCES

Ammler-von Eiff, M., & Guenther, E. W. 2009, A&A, 508, 677

Baraffe, I., Chabrier, G., Allard, F., & Hauschildt, P. H. 1998, A&A, 337, 403

Bean, J. L., et al. 2011, ApJ, 743, 92

Binks, A. S., & Jeffries, R. D. 2013, ArXiv e-prints

Bochanski, J. J., Hawley, S. L., Reid, I. N., Covey, K. R., West, A. A., Golimowski, D. A., & Ivezic, Z. 2008, ArXiv e-prints

Bonfils, X., et al. 2013, A&A, 549, A109, 75 pp

Bowler, B. P., Liu, M. C., Shkolnik, E. L., Dupuy, T. J., Cieza, L. A., Kraus, A. L., & Tamura, M. 2012, ApJ, 753, 142, 13 pp

Brandeker, A., Jayawardhana, R., & Najita, J. 2003, AJ, 126, 2009

Claire, M. W., Sheets, J., Cohen, M., Ribas, I., Meadows, V. S., & Catling, D. C. 2012, ApJ, 757, 95

de la Reza, R., Torres, C. A. O., Quast, G., Castilho, B. V., & Vieira, G. L. 1989, ApJ, 343, L61

Delfosse, X., et al. 2013, in SF2A-2013: Proceedings of the Annual meeting of the French Society of Astronomy and Astrophysics, ed. L. Cambresy, F. Martins, E. Nuss, & A. Palacios, 497–508

Delfosse, X., Forveille, T., Perrier, C., & Mayor, M. 1998, A&A, 331, 581

Deming, D., et al. 2009, PASP, 121, 952

Domagal-Goldman, S. D., Segura, A., Claire, M. W., Robinson, T. D., & Meadows, V. S. 2014, in Lunar and Planetary Science Conference, Vol. 45, Lunar and Planetary Science Conference, 2109

Dressing, C. D., & Charbonneau, D. 2014, in American Astronomical Society Meeting Abstracts, Vol. 223, American Astronomical Society Meeting Abstracts, 206.04

Feigelson, E. D., et al. 2004, ApJ, 611, 1107

Findeisen, K., & Hillenbrand, L. 2010, AJ, 139, 1338

Findeisen, K., Hillenbrand, L., & Soderblom, D. 2011, AJ, 142, 23

Fontenla, J. M., Curdt, W., Haberreiter, M., Harder, J., & Tian, H. 2009, ApJ, 707, 482

France, K., et al. 2013, ApJ, 763, 149

Gregorio-Hetem, J., Lepine, J. R. D., Quast, G. R., Torres, C. A. O., & de La Reza, R. 1992, AJ, 103, 549

Güdel, M., Guinan, E. F., & Skinner, S. L. 1997, ApJ, 483, 947

Guenther, E. W., Paulson, D. B., Cochran, W. D., Patience, J., Hatzes, A. P., & Macintosh, B. 2005, A&A, 442, 1031

Hauschildt, P. H., Baron, E., & Allard, F. 1997, ApJ, 483, 390

Hu, R., Seager, S., & Bains, W. 2012, ApJ, 761, 166

Irwin, J., Berta, Z. K., Burke, C. J., Charbonneau, D., Nutzman, P., West, A. A., & Falco, E. E. 2011, ApJ, 727, 56, 16 pp

Jackson, A. P., Davis, T. A., & Wheatley, P. J. 2012, MNRAS, 422, 2024

Jayawardhana, R., Coffey, J., Scholz, A., Brandeker, A., & van Kerkwijk, M. H. 2006, ApJ, 648, 1206

Kaltenegger, L., Segura, A., & Mohanty, S. 2011, ApJ, 733, 35

Kasting, J. F., Whitmire, D. P., & Reynolds, R. T. 1993, Icarus, 101, 108

Kopparapu, R. K. 2013, ApJ, 767, L8, 5 pp

Kopparapu, R. k., Kasting, J. F., & Zahnle, K. J. 2012, ApJ, 745, 77

Koskinen, T. T., Yelle, R. V., Lavvas, P., & Lewis, N. K. 2010, ApJ, 723, 116

Kraus, A. L., Shkolnik, E. L., Allers, K. N., & Liu, M. C. 2014, ArXiv e-prints

Kreidberg, L., et al. 2014, Nature, 505, 69

Kretzschmar, M., Dudok de Wit, T., Lilensten, J., Hochedez, J.-F., Aboudarham, J., Amblard, P.-O., Auchère, F., & Moussaoui, S. 2009, Acta Geophysica, 57, 42

Lammer, H., et al. 2007, Astrobiology, 7, 185

Lecavelier Des Etangs, A. 2007, A&A, 461, 1185

Lépine, S., & Gaidos, E. 2011, AJ, 142, 138

Lichtenegger, H. I. M., Lammer, H., Grießmeier, J.-M., Kulikov, Y. N., von Paris, P., Hausleitner, W., Krauss, S., & Rauer, H. 2010, Icarus, 210, 1

Line, M. R., Liang, M. C., & Yung, Y. L. 2010, ApJ, 717, 496

Linsky, J. L., Fontenla, J., & France, K. 2014, ApJ, 780, 61

Linsky, J. L., France, K., & Ayres, T. 2013, ApJ, 766, 69

Looper, D. L., et al. 2010, ApJ, 714, 45

López-Santiago, J., Montes, D., Crespo-Chacón, I., & Fernández-Figueroa, M. J. 2006, ApJ, 643, 1160

Malo, L., Doyon, R., Lafrenière, D., Artigau, É., Gagné, J., Baron, F., & Riedel, A. 2013, ApJ, 762, 88, 50 pp

Mandell, A. M., Raymond, S. N., & Sigurdsson, S. 2007, ApJ, 660, 823

Miguel, Y., & Kaltenegger, L. 2014, ApJ, 780, 166

Mitra-Kraev, U., et al. 2005, A&A, 431, 679

Montes, D., López-Santiago, J., Gálvez, M. C., Fernández-Figueroa, M. J., De Castro, E., & Cornide, M. 2001, MNRAS, 328, 45

Morrissey, P., et al. 2007, ApJS, 173, 682

—. 2005, ApJ, 619, L7

Moses, J. I., et al. 2013, ApJ, 777, 34

Ochsenbein, F., Bauer, P., & Marcout, J. 2000, A&AS, 143, 23

Pagano, I. 2009, Ap&SS, 320, 115

Perryman, M. A. C., et al. 1998, A&A, 331, 81

Perryman, M. A. C., & ESA, eds. 1997, ESA Special Publication, Vol. 1200, The HIPPARCOS and TYCHO catalogues. Astrometric and photometric star catalogues derived from the ESA HIPPARCOS Space Astrometry Mission

Pizzolato, N., Maggio, A., Micela, G., Sciortino, S., & Ventura, P. 2003, A&A, 397, 147

Pourbaix, D., et al. 2004, A&A, 424, 727

Poveda, A., Herrera, M. A., Allen, C., Cordero, G., & Lavalley, C. 1994, Rev. Mexicana Astron. Astrofis., 28, 43

Preibisch, T., & Feigelson, E. D. 2005, ApJS, 160, 390

Quirrenbach, A., et al. 2012, in Society of Photo-Optical Instrumentation Engineers (SPIE) Conference Series, Vol. 8446, Society of Photo-Optical Instrumentation Engineers (SPIE) Conference Series

Reid, N. 2003, MNRAS, 342, 837

Reiners, A., & Basri, G. 2009, A&A, 496, 787

Ricker, G. R., et al. 2014, ArXiv e-prints

Riedel, A. R., et al. 2014, AJ, 147, 85

Robinson, R. D., et al. 2005, ApJ, 633, 447

Robinson, T. D., Maltagliati, L., Marley, M. S., & Fortney, J. J. 2014, ArXiv e-prints

Rodriguez, D. R., Bessell, M. S., Zuckerman, B., & Kastner, J. H. 2011, ApJ, 727, 62

Sanz-Forcada, J., Micela, G., Ribas, I., Pollock, A. M. T., Eiroa, C., Velasco, A., Solano, E., & García-Álvarez, D. 2011, A&A, 532, A6, 18 pp

Scalo, J., et al. 2007, Astrobiology, 7, 85

Schmitt, J. H. M. M., Fleming, T. A., & Giampapa, M. S. 1995, ApJ, 450, 392

Segura, A., Kasting, J. F., Meadows, V., Cohen, M., Scalo, J., Crisp, D., Butler, R. A. H., & Tinetti, G. 2005, Astrobiology, 5, 706

Segura, A., Krelove, K., Kasting, J. F., Sommerlatt, D., Meadows, V., Crisp, D., Cohen, M., & Mlawer, E. 2003, Astrobiology, 3, 689

Segura, A., Walkowicz, L. M., Meadows, V., Kasting, J., & Hawley, S. 2010, Astrobiology, 10, 751

Selsis, F., Kasting, J. F., Levrard, B., Paillet, J., Ribas, I., & Delfosse, X. 2007, A&A, 476, 1373

Shkolnik, E., Liu, M. C., & Reid, I. N. 2009, ApJ, 699, 649

Shkolnik, E. L. 2013, ApJ, 766, 9

Shkolnik, E. L., Anglada-Escudé, G., Liu, M. C., Bowler, B. P., Weinberger, A. J., Boss, A. P., Reid, I. N., & Tamura, M. 2012, ApJ, 758, 56, 23 pp

Shkolnik, E. L., Liu, M. C., Reid, I. N., Dupuy, T., & Weinberger, A. J. 2011, ApJ, 727, 6, 12 pp

Short, C. I., & Hauschildt, P. H. 2005, ApJ, 618, 926

Skumanich, A. 1972, ApJ, 171, 565

Smith, G. H., & Redenbaugh, A. K. 2010, PASP, 122, 1303

Song, I., Zuckerman, B., & Bessell, M. S. 2003, ApJ, 599, 342

Stauffer, J. R., Balachandran, S. C., Krishnamurthi, A., Pinsonneault, M., Terndrup, D. M., & Stern, R. A. 1997, ApJ, 475, 604

Stelzer, B., Marino, A., Micela, G., López-Santiago, J., & Liefke, C. 2013, MNRAS, 431, 2063

—. 2014, MNRAS, 442, 343

Sterzik, M. F., Alcalá, J. M., Covino, E., & Petr, M. G. 1999, A&A, 346, L41

Tarter, J. C., et al. 2007, Astrobiology, 7, 30

Tian, F. 2009, ApJ, 703, 905

Tian, F., France, K., Linsky, J. L., Mauas, P. J. D., & Vieytes, M. C. 2014, Earth and Planetary Science Letters, 385, 22

Torres, C. A. O., Quast, G. R., da Silva, L., de La Reza, R., Melo, C. H. F., & Sterzik, M. 2006, A&A, 460, 695

Torres, C. A. O., Quast, G. R., Melo, C. H. F., & Sterzik, M. F. 2008, Young Nearby Loose Associations (Handbook of Star Forming Regions, Volume II: The Southern Sky ASP Monograph Publications, Vol. 5. Edited by Bo Reipurth), 757, 56 pp

Voges, W., et al. 1999, A&A, 349, 389

—. 2000, VizieR Online Data Catalog, 9029, 0

Walkowicz, L. M., Johns-Krull, C. M., & Hawley, S. L. 2008, ApJ, 677, 593

Webb, R. A., Zuckerman, B., Platais, I., Patience, J., White, R. J., Schwartz, M. J., & McCarthy, C. 1999, ApJ, 512, L63

Welsh, B. Y., et al. 2006, A&A, 458, 921

—. 2007, ApJS, 173, 673

Wheatley, P. J., et al. 2014, in IAU Symposium, Vol. 299, IAU Symposium, ed. M. Booth, B. C. Matthews, & J. R. Graham, 311–312

Woitke, P., et al. 2011, A&A, 534, A44, 27 pp

Wu, Y., & Lithwick, Y. 2013, ApJ, 772, 74, 13 pp

Zerkle, A. L., Claire, M. W., Domagal-Goldman, S. D., Farquhar, J., & Poulton, S. W. 2012, Nature Geoscience, 117, 359

Zuckerman, B., & Song, I. 2004, ARA&A, 42, 685

Zuckerman, B., Song, I., & Bessell, M. S. 2004, ApJ, 613, L65

Zuckerman, B., Webb, R. A., Schwartz, M., & Becklin, E. E. 2001, ApJ, 549, L233

This preprint was prepared with the AAS LaTeX macros v5.2.

Table 1. Target Early M Stars Observed by *GALEX*.

Name	R.A.$_{J2000}$ (deg.)	Dec.$_{J2000}$ (deg.)	SpT	J$_{2MASS}$ mag	Dist.[a] pc	Bin.[b] Type	Bin. Sep.[c] $''$	F_{FUV} μJy	F_{NUV} μJy	Refs.[d]
TW Hydra Association, 10 Myr old										
TWA 2 A	167.307540	-30.027720	M2	7.6	46.6	VB	0.5	38.18 ± 5.70	268.61 ± 10.12	1, 2
TWA 2 B	167.307540	-30.027720	M2	7.6	46.6	VB	0.5	38.18 ± 5.70	268.61 ± 10.12	1, 2
TWA 3 Aab	167.616200	-37.531100	M3	7.7	-34.0	VB, SB2	1.5	320.16 ± 19.77	961.84 ± 19.42	1, 2
TWA 3 B	167.616200	-37.531100	M3.5	7.7	-34.0	VB	1.5	320.16 ± 19.77	961.84 ± 19.42	1, 2
TWA 12	170.272917	-38.754722	M2	9.0	64.1	–	–	15.55 ± 5.86	82.10 ± 6.39	3, 2
TWA 13 B	170.321830	-34.779310	M2	8.4	55.6	VB	4.9	52.17 ± 7.12	321.75 ± 11.91	4, 4
TWA 13 A	170.322500	-34.780600	M1	8.4	55.6	VB	4.9	52.17 ± 7.12	321.75 ± 11.91	4, 4
TWA 5 Aab	172.980250	-34.607567	M1.5	7.7	50.1	VB+BD, SB2	2.5	65.22 ± 9.94	300.80 ± 11.17	5, 6
TWA 8 A	173.172900	-26.865300	M2-M3	8.3	-38.0	VB	13.7	41.84 ± 4.60	222.24 ± 4.43	7, 7
TWA 9 B	177.098870	-37.480140	M1	10.0	50.3	VB	5.9	26.86 ± 6.93	275.22 ± 11.32	7, 7
TWA 31[d]	181.795375	-32.514922	M4.2	13.0	80.0	–	–	28.82 ± 4.94	9.86 ± 3.49	8
TWA 23 ab	181.864080	-32.783420	M1	8.6	53.9	SB2	0.0	10.31 ± 3.96	53.33 ± 5.55	9, 8
TWA 20 ab	187.908620	-45.983170	M2	9.3	77.3	SB2	0.0	< 5.00	34.34 ± 5.20	10, 11
TWA 16	188.734583	-45.635453	M1.8	9.0	78.4	–	–	26.42 ± 7.03	56.14 ± 6.30	12
TWA 10	188.767710	-41.610720	M2.5	9.1	-53.0	–	–	5.98 ± 3.93	51.00 ± 5.47	7
TWA 30 B[d]	173.075929	-30.308792	M4	15.4	-42.0	VB	80.0	< 5.00	< 2.50	13, 13
β **Pic YMG, 12 Myr old**										
HIP 23418	75.494991	+09.983098	M3	7.2	32.1	–	–	226.04 ± 14.56	1010.39 ± 16.34	3
AT Mic B	310.462920	-32.436110	M4	5.8	10.2	VB	3.2	347.01 ± 15.70	1754.65 ± 14.87	3
AT Mic A	310.463350	-32.435280	M4	5.8	10.2	VB	3.2	347.01 ± 15.70	1754.65 ± 14.87	3
AU Mic	311.289580	-31.340830	M1	5.4	9.9	–	–	410.54 ± 13.47	2221.25 ± 19.69	3
LP 984-91	341.241509	-33.250484	M4.0	7.8	23.6	VB	35.5	29.28 ± 3.55	201.09 ± 5.92	9 & 14, 14
Tuc-Hor YMG. 40 Myr old										
HIP 1910	6.037500	-62.184440	M1	8.4	46.3	–	–	33.07 ± 5.69	152.52 ± 7.50	3
CT Tuc	6.311250	-61.513330	M1	8.6	37.5	–	–	16.72 ± 2.68	127.04 ± 4.92	3
HIP 3556	11.367317	-51.626090	M3	8.5	38.5	–	–	4.46 ± 2.04	38.03 ± 3.23	3
GSC 8056-0482	39.215438	-52.051011	M3	8.4	-25.0	–	–	23.91 ± 3.95	180.77 ± 5.70	3
AF Hor	40.447080	-52.991940	M2	8.5	-42.0	–	–	30.20 ± 3.59	136.69 ± 5.31	3
HIP 107345	326.125430	-60.977500	M1	8.8	42.3	–	–	18.53 ± 2.41	124.33 ± 3.18	3
TYC 9344-0293	351.544590	-73.397220	M0	8.8	-46.0	–	–	40.37 ± 6.26	129.09 ± 7.36	3
04133314-5231586	63.388090	-52.532970	M1.7	10.0	-47.2	–	–	Not. Obs.	4.26 ± 1.87	15
00514081-5913320	12.920050	-59.225580	M4.1	11.3	-41.3	–	–	< 3.00	1.70 ± 0.93	15
03114544-4719501	47.939350	-47.330590	M3.7	10.4	-33.1	–	–	< 3.00	7.11 ± 1.90	15

Table 1—Continued

Name	R.A.$_{J2000}$ (deg.)	Dec.$_{J2000}$ (deg.)	SpT	J$_{2MASS}$ mag	Dist.[a] pc	Bin.[b] Type	Bin. Sep.[c] $''$	F_{FUV} μJy	F_{NUV} μJy	Refs.[d]
01024375-6235344	15.682300	-62.592910	M3.8	9.6	-22.0	–	–	< 3.00	20.60 ± 2.51	15
23170011-7432095	349.250460	-74.535980	M4.1	10.4	-27.8	–	–	< 5.00	5.01 ± 2.61	15
04470041-5134405	71.751720	-51.577920	M2.4	10.1	-41.9	–	–	4.64 ± 1.67	13.02 ± 2.43	15
00485254-6526330	12.218950	-65.442520	M3.2	10.4	-39.1	–	–	< 5.00	10.01 ± 1.34	15
21504048-5113380	327.668680	-51.227250	M4.2	10.3	-25.9	–	–	3.53 ± 2.09	11.84 ± 2.07	15
21275054-6841033	321.960620	-68.684250	M4.1	10.4	-28.1	–	–	Not. Obs.	11.99 ± 0.84	15
00332438-5116433	8.351620	-51.278710	M2.4	9.9	-38.5	–	–	1.26 ± 1.48	17.71 ± 2.50	15
02341866-5128462	38.577790	-51.479510	M4.2	10.6	-29.4	–	–	5.94 ± 1.55	7.83 ± 1.96	15
02045317-5346162	31.221570	-53.771180	M3.4	10.4	-36.5	–	–	< 3.00	10.94 ± 2.19	15
23570417-0337559	359.267450	-03.632330	M3.3	10.9	-46.8	–	–	1.77 ± 0.53	6.35 ± 0.77	15
01283025-4921094	22.126080	-49.352630	M4.0	10.6	-31.3	–	–	< 3.00	13.15 ± 2.25	15
02321934-5746117	38.080610	-57.769940	M3.8	11.1	-42.7	–	–	< 5.00	7.39 ± 3.45	15
01160045-6747311	19.001910	-67.791980	M4.2	11.8	-49.4	–	–	< 3.00	1.67 ± 1.28	15
02590284-6120000	44.761850	-61.333350	M3.5	11.6	-60.3	–	–	< 3.00	3.45 ± 1.50	15
00394063-6224125	9.919300	-62.403480	M4.2	11.2	-39.1	–	–	Not. Obs.	7.57 ± 1.78	15
02001992-6614017	30.083040	-66.233830	M3.0	10.7	-49.4	–	–	3.28 ± 1.99	12.20 ± 1.38	15
01275875-6032243	21.994810	-60.540090	M4.0	11.1	-39.6	–	–	< 2.00	8.33 ± 1.63	15
04213904-7233562	65.412690	-72.565610	M2.4	9.9	-37.8	–	–	< 5.00	28.80 ± 2.93	15
02543316-5108313	43.638180	-51.142050	M1.4	8.7	-27.3	–	–	20.44 ± 3.32	83.31 ± 4.52	15
00273330-6157169	6.888760	-61.954720	M3.5	10.3	-33.9	–	–	< 5.00	20.07 ± 3.38	15
00152752-6414545	3.864670	-64.248500	M1.5	9.3	-36.3	–	–	13.26 ± 3.27	39.69 ± 4.51	15
22223966-6303258	335.665290	-63.057180	M3.2	10.2	-35.3	–	–	4.77 ± 2.25	23.28 ± 3.81	15
02242453-7033211	36.102240	-70.555890	M4.0	10.4	-28.3	–	–	< 3.00	13.53 ± 1.65	15
03291649-3702502	52.318740	-37.047280	M3.7	10.7	-36.1	–	–	2.63 ± 1.59	11.79 ± 3.10	15
00493566-6347416	12.398610	-63.794900	M1.8	9.3	-33.6	–	–	9.04 ± 2.76	46.93 ± 3.59	15
23291752-6749598	352.323020	-67.833300	M3.9	10.8	-35.6	–	–	3.08 ± 1.46	9.64 ± 1.36	15
02502222-6545552	42.592620	-65.765360	M2.8	10.3	-42.1	–	–	2.87 ± 2.07	17.07 ± 2.36	15
02070176-4406380	31.757340	-44.110570	M1.2	9.3	-37.5	–	–	7.86 ± 1.97	53.39 ± 2.84	15
04133609-4413325	63.400410	-44.225700	M3.3	10.77	-44.5	–	–	< 5.00	12.63 ± 3.21	15
21143354-4213528	318.639790	-42.231350	M4.1	11.4	-43.5	–	–	< 5.00	7.34 ± 1.27	15
00235732-5531435	5.988860	-55.528770	M4.0	11.1	-40.4	–	–	< 5.00	8.77 ± 2.61	15
02474639-5804272	41.943320	-58.074220	M1.6	9.4	-35.5	–	–	11.85 ± 2.25	51.98 ± 3.65	15
00421010-5444431	10.542090	-54.745310	M3.0	9.8	-31.6	–	–	8.80 ± 2.38	36.27 ± 2.89	15
22244102-7724036	336.170920	-77.401020	M4.0	11.4	-45.9	–	–	< 3.00	8.04 ± 1.79	15

Table 1—Continued

Name	R.A.$_{J2000}$ (deg.)	Dec.$_{J2000}$ (deg.)	SpT	J$_{2MASS}$ mag	Dist.[a] pc	Bin.[b] Type	Bin. Sep.[c] $''$	F_{FUV} μJy	F_{NUV} μJy	Refs.[d]
02001277-0840516	30.053270	-08.681140	M2.0	8.8	-25.4	–	–	22.34 ± 0.96	96.91 ± 1.68	15
01224511-6318446	20.687960	-63.312390	M3.3	9.8	-28.7	–	–	6.65 ± 3.05	39.08 ± 3.48	15
22463471-7353504	341.644660	-73.897350	M3.2	9.66	-27.5	–	–	Not. Obs.	42.93 ± 1.16	15
22021626-4210329	330.567750	-42.175830	M0.8	8.93	-33.3	–	–	18.48 ± 2.59	84.09 ± 2.97	15
01351393-0712517	23.808040	-07.214380	M4.1	8.96	-14.2	–	–	17.44 ± 3.60	87.83 ± 4.65	15
01505688-5844032	27.737030	-58.734230	M2.9	9.54	-28.3	–	–	9.13 ± 2.74	47.93 ± 3.76	15
02205139-5823411	35.214130	-58.394760	M3.2	9.7	-27.8	–	–	10.99 ± 3.64	40.23 ± 3.95	15
02505959-3409050	42.748330	-34.151410	M3.8	10.5	-32.5	–	–	< 5.00	23.52 ± 3.54	15
00125703-7952073	3.237660	-79.868700	M3.4	9.7	-25.4	–	–	Not. Obs.	46.29 ± 4.08	15
23474694-6517249	356.945610	-65.290260	M1.5	9.1	-32.2	–	–	13.60 ± 3.97	80.38 ± 5.55	15
03050976-3725058	46.290700	-37.418280	M2.5	9.54	-31.6	–	–	7.45 ± 2.30	53.02 ± 3.85	15
03210395-6816475	50.266470	-68.279870	M3.4	10.36	-33.4	–	–	7.18 ± 2.51	22.15 ± 3.52	15
22025453-6440441	330.727230	-64.678920	M2.1	9.1	-28.3	–	–	13.90 ± 2.84	84.82 ± 4.16	15
21163528-6005124	319.147040	-60.086780	M3.9	10.2	-27.0	–	–	6.97 ± 2.21	28.90 ± 2.52	15
20423672-5425263	310.653010	-54.423990	M3.9	10.8	-35.2	–	–	5.13 ± 2.00	16.56 ± 1.86	15
00240899-6211042	6.037490	-62.184520	M0.2	8.4	-28.6	–	–	33.07 ± 5.69	152.52 ± 7.50	15
23452225-7126505	356.342720	-71.447380	M3.8	10.2	-28.3	–	–	3.91 ± 1.77	29.35 ± 3.05	15
01211297-6117281	20.304080	-61.291150	M4.1	11.3	-42.3	–	–	< 5.00	9.78 ± 3.52	15
23273447-8512364	351.893630	-85.210130	M4.0	10.9	-35.8	–	–	< 3.00	16.04 ± 2.52	15
01521830-5950168	28.076260	-59.838000	M1.6	8.9	-30.3	–	–	25.25 ± 3.68	100.47 ± 4.54	15
21443012-6058389	326.125500	-60.977500	M0.0	8.8	-34.8	–	–	18.53 ± 2.41	124.33 ± 3.18	15
03315564-4359135	52.981850	-43.987110	M0.0	8.3	-28.4	–	–	20.84 ± 4.02	187.51 ± 6.19	15
00144767-6003477	3.698650	-60.063260	M3.5	9.71	-25.1	–	–	8.53 ± 3.42	50.09 ± 4.72	15
21370885-6036054	324.286880	-60.601520	M3.6	9.6	-23.4	–	–	9.72 ± 2.56	62.20 ± 2.36	15
02125819-5851182	33.242490	-58.855060	M3.5	9.3	-21.0	–	–	24.21 ± 5.36	81.45 ± 4.96	15
23261069-7323498	351.544540	-73.397190	M1.5	8.8	-28.7	–	–	40.37 ± 6.26	129.09 ± 7.36	15
02420404-5359000	40.516860	-53.983350	M3.9	10.1	-26.7	–	–	16.68 ± 4.24	36.13 ± 4.68	15
05392505-4245211	84.854380	-42.755890	M1.8	9.5	-36.1	–	–	6.60 ± 3.28	73.66 ± 5.67	15
23285763-6802338	352.240160	-68.042750	M2.9	9.3	-25.4	–	–	23.52 ± 3.25	90.08 ± 2.62	15
23131671-4933154	348.319620	-49.554300	M4.1	9.76	-20.7	–	–	12.03 ± 2.56	59.29 ± 3.52	15
02423301-5739367	40.637550	-57.660200	K7.1	8.6	-40.7	–	–	21.18 ± 3.40	173.90 ± 5.23	15
02303239-4342232	37.635000	-43.706470	K7.0	8.02	-32.4	–	–	11.13 ± 3.53	308.04 ± 8.94	15
00393579-3816584	9.899160	-38.282890	M1.8	8.8	-26.3	–	–	27.23 ± 3.91	163.64 ± 6.08	15
04365738-1613065	69.239100	-16.218490	M3.0	9.1	-22.9	–	–	36.06 ± 4.53	125.45 ± 5.10	15

Table 1—Continued

Name	R.A.$_{J2000}$ (deg.)	Dec.$_{J2000}$ (deg.)	SpT	J$_{2MASS}$ mag	Dist.[a] pc	Bin.[b] Type	Bin. Sep.[c] $''$	F_{FUV} μJy	F_{NUV} μJy	Refs.[d]
21100614-5811483	317.525620	-58.196750	M3.8	10.9	-39.6	–	–	< 5.00	24.12 ± 3.89	15
04074372-6825111	61.932190	-68.419770	M2.6	10.4	-46.6	–	–	12.74 ± 2.71	57.57 ± 3.89	15
23382851-6749025	354.618810	-67.817370	M3.9	10.9	-37.8	–	–	20.75 ± 3.12	42.17 ± 2.27	15
03244056-3904227	51.169030	-39.072980	M4.1	9.9	-21.7	–	–	26.80 ± 3.85	114.95 ± 4.85	15
04000382-2902165	60.015920	-29.037930	K7.2	8.0	-30.3	–	–	85.70 ± 8.31	663.68 ± 14.71	15
05111098-4903597	77.795750	-49.066600	M3.7	10.6	-35.8	–	–	43.23 ± 7.13	70.95 ± 3.20	15
AB Dor YMG. 100 Myr old										
CD-61 1439	99.958340	-61.478330	K7	7.3	21.9	–	–	25.51 ± 3.15	319.08 ± 6.79	3
BD+01 2447	157.231670	+00.841110	M2.5	6.2	7.2	–	–	10.20 ± 0.81	101.36 ± 1.73	16
HD 201919	318.272090	-17.486940	K6	8.3	22.6	–	–	30.07 ± 4.76	227.13 ± 6.63	6
HD 217379	345.116670	-26.311940	K7	7.0	30.0	–	–	37.48 ± 4.16	392.79 ± 5.32	3
G 132-51 B (W)	15.925539	+40.854309	M2.6	–	31.3	VB	0.6	12.97 ± 3.59	45.96 ± 5.02	14, 14
G 132-51 B (E)	15.925539	+40.854309	M3.8	–	31.3	VB	0.6	12.97 ± 3.59	45.96 ± 5.02	14, 14
GJ 3136	32.223427	+49.449021	M2.9	8.4	15.5	–	–	18.12 ± 5.74	124.20 ± 5.92	14, 14
G 80-21	56.847252	-01.972217	M2.8	7.8	16.3	–	–	Not. Obs.	150.45 ± 8.61	17 & 14
NLTT 14116	73.101689	-16.822761	M3.3	7.7	16.3	–	–	82.56 ± 7.49	232.17 ± 7.31	14
NLTT 15049 A (SW)	81.423609	-09.153466	M3.8	8.5	20.7	VB	0.5	Not. Obs.	61.96 ± 7.89	14, 14 & 18
BD+20 1790	110.931622	+20.416288	K7	7.6	25.8	–	–	46.40 ± 6.22	568.68 ± 12.67	14
GJ 4231	328.043385	+05.626629	M2.4	8.2	31.8	–	–	32.29 ± 5.68	177.54 ± 7.94	14
GJ 9809	346.520188	+63.926213	M0.3	7.8	24.9	–	–	Not. Obs.	276.41 ± 13.96	19 & 14
1RXS J235133.3+312720 AB	357.890302	+31.456391	M2.0	9.8	45.0	VB (with BD)	2.4	11.71 ± 2.59	42.71 ± 3.15	14, 20
HIP 110526	56.847252	-01.972217	M3	7.8	16.3	–	–	Not. Obs.	153.15 ± 8.13	3
Ursa Major Association, 300 Myr old										
2MASS J10364483+1521394 A (N)	159.186857	+15.360932	M4	8.7	20.1	VB	1.0	14.51 ± 1.07	60.77 ± 1.53	14, 14
HD 95650	165.659764	+21.967136	M2	6.5	11.7	–	–	53.21 ± 8.27	367.94 ± 11.46	21
1RXS J111300.1+102518	168.252503	+10.418295	M3.0	10.0	23.0	–	–	< 5.00	29.33 ± 4.09	14
G 10-52	177.147885	+07.694533	M3.5	9.5	20.7	–	–	11.33 ± 3.11	34.35 ± 3.17	14
GJ 4381 AB	359.457703	+38.629529	M2.8	8.7	-21.3	VB	0.5	31.62 ± 3.74	81.09 ± 3.28	14, 14
Hyades Cluster, 650 Myr old										
LP 247-13	48.907641	+37.403984	M2.7	9.3	34.4	–	–	15.15 ± 5.55	67.99 ± 6.08	14
1RXS J032230.7+285852	50.631912	+28.974766	M4.0	10.8	46.7	–	–	< 5.00	19.28 ± 4.32	14
Cl* Melotte 25 REID 187	65.849178	+14.427931	M2.5	10.5	46.3	–	–	1.86 ± 1.24	16.27 ± 1.04	22
Cl* Melotte 25 HAN 366	66.460166	+15.002594	M4	11.6	46.3	–	–	Not. Obs.	2.49 ± 0.73	22
TYC 1265-1118-1	66.519614	+15.041349	M1	9.3	46.3	–	–	1.15 ± 0.75	24.75 ± 1.05	22

Table 1—Continued

Name	R.A.$_{J2000}$ (deg.)	Dec.$_{J2000}$ (deg.)	SpT	J$_{2MASS}$ mag	Dist.[a] pc	Bin.[b] Type	Bin. Sep.[c] $''$	F_{FUV} μJy	F_{NUV} μJy	Refs.[d]
Cl* Melotte 25 REID 228	66.517985	+17.120720	M3	10.9	46.3	–	–	15.23 ± 0.45	20.00 ± 0.36	22
V1102 Tau	67.119925	+17.695940	M1	8.6	46.3	VB	1.6	35.85 ± 7.00	115.38 ± 8.34	22, 23
Cl* Melotte 25 REID 277	67.477499	+16.912815	M2	–	46.3	–	–	< 1.00	1.63 ± 0.38	22
V484 Tau	67.599799	+17.499760	M3.5	10.4	46.3	–	–	< 3.00	18.03 ± 2.72	22
GSC 01269-00867	67.871049	+17.718683	M1	9.1	46.3	–	–	Not. Obs.	35.25 ± 4.67	22
Cl* Melotte 25 REID 306	68.033131	+17.664526	M2	10.9	46.3	–	–	Not. Obs.	< 2.00	22
Cl* Melotte 25 HAN 530	68.120746	+17.904619	M4	11.2	46.3	–	–	Not. Obs.	16.71 ± 3.53	22
Cl* Melotte 25 HAN 172	64.448646	+13.661744	M1	9.4	46.3	VB	0.8	< 3.00	13.08 ± 2.10	22, 23
Melotte 25 HAN 192	64.695927	+13.366275	M1	9.1	46.3	–	–	< 6.00	20.69 ± 2.50	22
Melotte 25 REID 189	65.928942	+15.880928	M2	10.7	46.3	–	–	< 2.00	1.40 ± 0.75	22
LP 415-1582	69.017367	+18.888599	M3.5	9.8	46.3	–	–	26.31 ± 4.39	51.27 ± 2.89	22
LP 415-1619	69.162224	+18.615774	M3	9.8	46.3	–	–	< 5.00	5.30 ± 1.58	22
LP 15-292	69.727959	+19.182240	M3	10.2	46.3	–	–	< 5.00	27.03 ± 2.08	22
Cl Melotte 25 310	70.052960	+19.286110	M1	9.9	46.3	–	–	< 5.00	3.91 ± 1.20	22
Cl* Melotte 25 REID 122	64.005982	+16.983133	M1	10.8	46.3	–	–	< 3.00	5.62 ± 2.12	22
Cl* Melotte 25 REID 132	64.180400	+16.822313	M3	11.2	46.3	–	–	< 3.00	6.01 ± 2.72	22
Cl* Melotte 25 REID 142	64.479131	+16.544498	M2	10.0	46.3	–	–	7.04 ± 3.12	34.11 ± 3.47	22
GJ 3290	66.819316	+17.241827	M1.5	9.7	46.3	–	–	< 3.00	7.68 ± 3.08	22
Cl* Melotte 25 VA 559	67.482176	+16.914061	M2	9.5	46.3	–	–	3.45 ± 0.42	25.69 ± 0.40	22
LP 358-534	65.482731	+23.418280	M4	9.9	46.3	–	–	< 1.00	11.30 ± 1.78	22
LP 358-724	66.325686	+23.060841	M4	10.3	46.3	–	–	Not. Obs.	< 2.00	22
Cl* Melotte 25 REID 135	64.226897	+16.356930	M4	10.4	46.3	–	–	< 3.00	2.16 ± 2.01	22
1RXS J041755.6+163249	64.479131	+16.544498	M3	10.0	46.3	–	–	14.08 ± 4.25	31.42 ± 2.76	22
Cl* Melotte 25 REID 176	65.664747	+18.269377	M0.5	9.6	46.3	–	–	Not. Obs.	2.15 ± 1.79	22
1RXS J042829.4+174138	67.122875	+17.694851	M2	–	46.3	–	–	35.85 ± 7.00	115.38 ± 8.34	22
Field sample, ∼5 Gyr old										
Gl 1	1.351785	-37.357361	M1.5	5.3	4.3	–	–	< 3.00	49.93 ± 2.38	24
Gl 48	15.634300	+71.679816	M3.0	6.3	8.2	–	–	6.62 ± 2.16	66.77 ± 4.64	24
Gl 49	15.661952	+62.345048	M1.5	6.2	10.0	–	–	Not. Obs.	226.49 ± 11.82	24
Gl 54	17.595428	-67.444959	M2.0	6.0	8.2	–	–	7.42 ± 2.27	71.25 ± 3.97	24
Gl 84	31.270188	-17.614637	M2.5	6.5	9.1	–	–	10.47 ± 2.68	52.20 ± 5.06	24
GJ 3135	31.452312	-30.176639	M2.5	8.4	9.3	–	–	Not. Obs.	< 4.65	24
Gl 109	41.064621	+25.523364	M3.0	6.8	7.5	–	–	< 3.00	29.77 ± 3.33	24
GJ 3193 B	45.464123	-16.593364	M3.0	7.3	9.4	VB	7.1	25.53 ± 1.32	95.91 ± 1.60	24, 25

Table 1—Continued

Name	R.A.$_{J2000}$ (deg.)	Dec.$_{J2000}$ (deg.)	SpT	J$_{2MASS}$ mag	Dist.[a] pc	Bin.[b] Type	Bin. Sep.[c] $''$	F_{FUV} μJy	F_{NUV} μJy	Refs.[d]
GJ 1065	57.684670	-06.094440	M3.5	8.6	9.5	–	–	< 2.00	5.89 ± 1.16	24
Gl 176	70.732396	+18.958168	M2.0	6.5	9.3	–	–	10.68 ± 4.09	126.10 ± 5.13	24
GJ 3325	75.833690	-17.373539	M3.0	7.8	9.2	–	–	< 3.00	10.81 ± 2.42	24
Gl 191	77.919088	-45.018414	M1.0	5.8	3.9	–	–	< 5.00	< 2.00	24
GJ 3378	90.296104	+59.597450	M3.5	7.5	7.9	–	–	< 3.00	< 2.00	24
Gl 226	92.582703	+82.106756	M2.0	6.9	9.4	–	–	0.34 ± 1.84	36.57 ± 3.13	24
Gl 257 A	104.447758	-44.291131	M3.0	6.9	8.0	VB	1.5	Not. Obs.	< 3.00	24, 25
Gl 273	111.852082	+05.225787	M3.5	5.7	3.8	–	–	7.60 ± 2.25	32.34 ± 3.68	24
GJ 1105	119.552907	+41.303690	M3.5	7.7	8.6	–	–	11.44 ± 2.62	27.17 ± 3.56	24
GJ 2066	124.033260	+01.302573	M2.0	6.6	9.1	–	–	< 6.00	53.23 ± 3.89	24
GJ 3522	134.734710	+08.473860	M3.5	6.5	6.8	ABC (SB+C)	0.6	104.68 ± 1.66	376.21 ± 2.00	24, 26
GJ 1125	142.685764	+00.322657	M3.5	7.7	9.7	–	–	< 3.00	11.92 ± 2.46	24
Gl 358	144.943205	-41.067558	M2.0	6.9	9.5	–	–	8.81 ± 5.29	Not Obs.	24
Gl 367	146.124322	-45.776508	M1.0	6.6	9.9	–	–	24.23 ± 5.31	Not Obs.	24
Gl 382	153.073621	-03.745666	M1.5	5.9	7.9	–	–	18.70 ± 2.81	220.52 ± 6.50	24
Gl 393	157.231462	+00.841006	M2.0	6.2	7.1	–	–	10.20 ± 0.81	101.36 ± 1.73	24
Gl 408	165.017737	+22.832958	M2.5	6.3	6.7	–	–	4.32 ± 2.34	53.59 ± 4.82	24
Gl 411	165.834142	+35.969880	M2.0	4.2	2.6	–	–	30.10 ± 5.48	468.13 ± 11.11	24
Gl 412 A	166.369075	+43.526775	M0.5	5.5	4.9	VB (+M6)	35.7	15.94 ± 1.22	50.66 ± 1.41	24, 25
Gl 424	170.020119	+65.846485	M0.0	6.3	8.9	–	–	< 5.00	131.53 ± 7.33	24
Gl 433	173.862278	-32.539971	M1.5	6.5	8.9	–	–	Not. Obs.	66.23 ± 6.19	24
Gl 445	176.922406	+78.691163	M3.5	6.7	5.4	–	–	< 3.00	10.82 ± 1.85	24
Gl 450	177.780572	+35.272015	M1.0	6.4	8.6	–	–	8.43 ± 3.32	110.79 ± 7.01	24
Gl 465	186.218762	-18.242290	M2.0	7.7	8.9	–	–	< 3.00	< 2.00	24
Gl 480.1	190.192871	-43.566376	M3.0	8.2	7.8	–	–	< 5.00	< 2.50	24
Gl 514	202.499109	+10.377164	M0.5	5.9	7.7	–	–	< 5.00	177.59 ± 6.73	24
GJ 3801	205.680292	+33.290099	M3.5	7.8	9.3	–	–	< 5.00	3.38 ± 2.61	24
Gl 581	229.864621	-07.722067	M3.0	6.7	6.2	–	–	< 1.00	< 1.00	24
Gl 623	246.038854	+48.352906	M2.5	6.6	8.1	–	–	7.90 ± 2.17	53.00 ± 2.71	24
Gl 625	246.352597	+54.304104	M1.5	6.6	6.5	–	–	< 3.00	36.78 ± 2.25	24
GJ 1207	254.273790	-04.348890	M3.5	8.0	8.7	–	–	32.15 ± 1.74	105.01 ± 0.41	24
GJ 3991	257.381434	+43.681341	M3.5	7.4	7.5	–	–	8.23 ± 2.48	58.86 ± 4.84	24
Gl 678.1 A	262.594696	+05.548531	M0.0	6.2	10.0	VB	16.4	14.12 ± 3.21	149.02 ± 3.95	24, 25
Gl 682	264.265260	-44.319214	M3.5	6.5	5.1	–	–	Not. Obs.	13.00 ± 4.44	24

Table 1—Continued

Name	R.A.$_{J2000}$ (deg.)	Dec.$_{J2000}$ (deg.)	SpT	J$_{2MASS}$ mag	Dist.[a] pc	Bin.[b] Type	Bin. Sep.[c] $''$	F_{FUV} μJy	F_{NUV} μJy	Refs.[d]
Gl 686	264.472279	+18.591711	M1.0	6.4	8.1	–	–	< 5.00	90.85 ± 3.60	24
Gl 694	265.983178	+43.378610	M2.5	6.8	9.5	–	–	< 5.00	33.23 ± 3.50	24
Gl 693	266.642624	-57.319043	M2.0	6.9	5.8	–	–	< 6.00	7.33 ± 3.85	24
Gl 701	271.281579	-03.031322	M1.0	6.2	7.8	–	–	Not. Obs.	98.13 ± 6.67	24
Gl 725 A	280.694497	+59.630409	M3.0	5.2	3.6	VB	13.3	22.86 ± 3.54	130.05 ± 6.00	24, 25
Gl 725 B	280.695694	+59.626763	M3.5	5.7	3.5	VB	13.3	< 3.00	36.07 ± 3.69	24, 25
Gl 729	282.455676	-23.836230	M3.5	6.2	3.0	–	–	67.53 ± 6.15	290.53 ± 7.53	24
Gl 745 A	286.773180	+20.888046	M1.5	7.3	8.5	VB	114.2	< 5.00	15.57 ± 3.00	24, 25
Gl 745 B	286.805013	+20.877011	M2.0	7.3	8.8	VB	114.2	< 5.00	16.73 ± 3.12	24, 25
Gl 793	307.633520	+65.449558	M2.5	6.7	8.0	–	–	< 5.00	78.55 ± 5.13	24
Gl 809	313.332460	+62.154390	M0.5	5.4	7.1	–	–	Not. Obs.	349.48 ± 9.95	24
Gl 829	322.403384	+17.643293	M3.5	6.2	6.7	–	–	< 5.00	40.20 ± 3.15	24
Gl 832	323.391564	-49.009005	M1.5	5.3	5.0	–	–	20.85 ± 2.98	176.59 ± 5.32	24
GJ 4248	330.622304	-37.080894	M3.5	7.6	7.5	–	–	Not. Obs.	13.27 ± 3.60	24
Gl 867 AabC	339.689894	-20.621134	M1.5	5.7	8.7	SB+VB	24.5	234.46 ± 10.69	1303.88 ± 15.04	24, 27
Gl 877	343.939623	-75.458669	M2.5	6.6	8.6	–	–	5.25 ± 1.81	42.24 ± 2.97	24
Gl 880	344.145020	+16.553432	M1.5	5.4	6.8	–	–	15.23 ± 3.30	347.39 ± 8.22	24
Gl 908	357.302200	+02.401224	M1.0	5.8	6.0	–	–	13.55 ± 2.40	130.30 ± 5.16	24

[a]Distances are from Hipparcos (Perryman & ESA 1997). Those with negative signs in front are photometric distances based on Baraffe et al. (1998) models. Hyades members without individual Hipparcos measurements are assumed to have the cluster distance of 46.34 ± 0.27 pc from Perryman et al. (1998).

[b]VB = visual binary and SB = spectroscopic binary.

[c]Binaries with separations $<35''$ are not resolved by *GALEX*.

[d]References for group members and binarity, e.g. X, Y. These are: 1: de la Reza et al. (1989) , 2: Brandeker et al. (2003), 3: Zuckerman & Song (2004), 4: Sterzik et al. (1999), 5: Gregorio-Hetem et al. (1992), 6: Torres et al. (2006), 7: Webb et al. (1999), 8: Shkolnik et al. (2011), 9: Song et al. (2003), 10: Reid (2003), 11: Jayawardhana et al. (2006), 12: Zuckerman et al. (2001), 13: Looper et al. (2010), 14: Shkolnik et al. (2012), 15: Kraus et al. (2014), 16: Montes et al. (2001), 17: Zuckerman et al. (2004), 18: Malo et al. (2013), 19: López-Santiago et al. (2006), 20: Bowler et al. (2012), 21: Ammler-von Eiff & Guenther (2009), 22: Perryman et al. (1998), 23: Guenther et al. (2005), 24: Lépine & Gaidos (2011), 25: Poveda et al. (1994), 26: Riedel et al. (2014), 27: Pourbaix et al. (2004).

[d]TWA 31 and TWA 30 B are both known to be accretors from Shkolnik et al. (2011) and Looper et al. (2010), respectively. TWA 30 B's J-band flux is also extincted, and thus is not included in the analysis.

Table 2. Power-law coefficients for $y \propto x^{\beta}$

x	y	Subset	β	R	#
$(F_{NUV}/F_J)_{exc}$	$(F_{FUV}/F_J)_{exc}$	all	1.11 ± 0.04	0.93	121
$(F_{NUV}/F_J)_{exc}$	$(F_{FUV}/F_J)_{exc}$	strong emitters only	1.00 ± 0.08	0.79	102
F_{NUV}/F_J	NUV surface flux	those with parallaxes	1.05 ± 0.04	0.94	103
F_{FUV}/F_J	FUV surface flux	those with parallaxes	0.96 ± 0.05	0.91	72
F_X/F_J	$(F_{FUV}/F_J)_{exc}$	all	0.73 ± 0.06	0.85	65
F_X/F_J	$(F_{NUV}/F_J)_{exc}$	all	0.61 ± 0.05	0.83	65
F_X/F_J	$(F_{FUV}/F_J)_{exc}$	strong emitters only	0.41 ± 0.13	0.42	53
F_X/F_J	$(F_{NUV}/F_J)_{exc}$	strong emitters only	0.35 ± 0.12	0.36	53
F_X/F_J	$(F_{FUV}/F_J)_{exc}$	weak emitters only	0.34 ± 0.20	0.49	12
F_X/F_J	$(F_{NUV}/F_J)_{exc}$	weak emitters only	0.13 ± 0.23	0.18	53
Age	F_X/F_J	medians, $\gtrsim$300 Myr	-1.36 ± 0.32	-0.97	3
Age	$(F_{FUV}/F_J)_{exc}$	medians, $\gtrsim$300 Myr	-0.99 ± 0.19	-0.98	3
Age	$(F_{NUV}/F_J)_{exc}$	medians, $\gtrsim$300 Myr	-0.84 ± 0.09	-0.99	3